On the effect of islands in the diffusive properties of the standard map, for large parameter values

Narcís Miguel, Carles Simó and Arturo Vieiro

Dept. de Matemàtica Aplicada i Anàlisi, Universitat de Barcelona, Gran Via 585, 08007, Barcelona, Catalunya

narcis@maia.ub.es carles@maia.ub.es vieiro@maia.ub.es

Abstract

In this paper we review, based on massive, long term, numerical simulations, the effect of islands on the statistical properties of the standard map for large parameter values. Different sources of discrepancy with respect to typical diffusion are identified, the individual roles of them are compared and explained in terms of available limit models.

To Mike Shub, on his 70th anniversary, with our best wishes and as a recognition to his great mathematical achievements

Mathematics Subject Classification: Primary: 37A50; Secondary: 37D45, 37J99, 37M99
Keywords: standard map, accelerator modes, diffusion, stickiness

1 Introduction

One of the main goals of Dynamical Systems is the description, explanation and prediction of the properties of the orbits of a given system. In some cases the individual orbits behave in a seemingly random way, with different properties in different domains of the phase space.

This occurs already in simple models, like area preserving maps. One of the typical models which displays many of the general properties of this class of maps is the Chirikov standard map [1]. For large enough values of the parameter the behavior of the orbits seems like a diffusive process. But this is far from being true for some ranges of the parameter, as noticed by many authors in the past (see references in the Bibliography).

The purpose of the present work is to present the results of massive simulations for large sets of values of the parameter and to explain the different phenomena that lead to the destruction of the diffusive character. This is done using quantitative and qualitative approaches. The results are compared to some limit theoretical models which deal with several of the involved phenomena.

In Section 2 we review, first, some properties of the Hénon conservative map [14]. As it will be shown in Section 3, devoted to describe some key properties of the standard map, the Hénon map is quite useful to understand more general area preserving maps. In particular, it clarifies the strong changes in the behaviour of the diffusion in the standard map.

Simple approaches to the diffusive properties of the standard map are considered in Section 4: the quasi-linear approximation and the Fourier methods to take into account the correlation effects. These methods are useful for many of the values of the parameter when it is large enough.

Section 5 is devoted to methods and results obtained from massive simulations. After looking at the problem for a large set of values of the parameter, we consider narrower and narrower ranges to focus on the main difficulties. A scaling effect shows up and, hence, details on the dynamics in a narrow parameter domain allow us to understand the behavior at all the other places where the standard diffusion is no longer valid.

Quantitative and qualitative explanations of the numerical results, as well as a comparison with limit renormalization schemes are the contents of Section 6. The main result concerns the behaviour of the standard deviation of the iterates of points, initially in a given ensemble in the chaotic domain, as a function of the number of iterates T. While for a typical diffusive process it behaves as the square root of T, for some intervals, in the domain of large parameter values, it behaves as a larger power of T, whose exponents range, approximately, between 0.7 and 1.

A description of what the orbits do, which explains the main features of the plots which summarize the numerical results, is presented at the end of Section 6.4.

The topic discussed in this paper is a very popular one and has a large amount of contributions and theoretical discussions. Anyway there are still many open questions. In particular, it is not known if microscopic islands occupy a large part of what can seem to be a chaotic domain in the phase space. The results of Duarte [6] show that there is a residual set of large enough parameters in the standard map for which any point is at a small distance of an elliptic periodic point, the distance tending to zero when the parameter tends to infinity. The existence of these elliptic points follows from homoclinic tangencies and a conservative version of Newhouse theorem.

In this context it appears the problem of the positiveness of the metric entropy as one of the key problems. It is not known a single value of the parameter of the standard map for which the metric entropy has been proved to be positive. In particular, it has not been proved that the set of points with positive Lyapunov exponent has positive measure, a fact which would imply positive metric entropy thanks to Pesin's work [34]. The problem becomes more tractable if some amount of noise is added to the deterministic conservative map, see [18].

This contribution has to be seen as an attempt to find quantitative explanations to the results of a large number of simulations, so that one could find the main theoretical reasons which allow to predict, accurately, which should be the observed behaviour of the diffusive properties of the standard map for some special ranges, near integer values, when the parameter is large.

2 A summary of properties of the Hénon conservative orientation-preserving map

The well-known Hénon map,

$$F : (x, y) \to (1 - ax^2 + y, bx), \qquad a, b \in \mathbb{R}\,, \tag{1}$$

is the simplest map with nontrivial dynamics in $\mathbb{R}^2$. In turn, generic (in fact, almost all) quadratic maps in $\mathbb{R}^2$ with constant Jacobian can be reduced to (1). For $b = \pm 1$ it preserves area: for $b = -1$ it also preserves orientation and for $b = 1$ it reverses it.

For the case $b = -1$, a parameter depending change of variables [40] gives us a more suitable representation of (1) for our purposes,

$$HP_c : \begin{pmatrix} x \\ y \end{pmatrix} \to \begin{pmatrix} c(1 - x^2) + 2x + y \\ -x \end{pmatrix}. \tag{2}$$

Here HP stands for Hénon orientation preserving, and the subscript c is added to stress out the explicit dependence on the parameter c. It is enough to consider $c > 0$. The map (2) has two fixed points, whose position in the plane does not depend on $c :$ a hyperbolic fixed point for $c > 0$ at $(-1, 1)$ and an elliptic fixed point at $(1, -1)$. Last one is elliptic for $0 < c < 2$, parabolic for $c = 2$ and reflection hyperbolic for $c > 2$.

The orientation-preserving Hénon map is recovered as a universal return map that approximates the local dynamics around a periodic orbit created at the unfolding of a quadratic tangency of a general area-preserving map, see for example [12] and references therein for details. Also the orientation-reversing Hénon map, that will be introduced later in Section 3.2, appears as a universal return map in non-orientable cases, either for maps defined in non-orientable manifolds or for hyperbolic points with eigenvalues λ and μ such that $\lambda\mu = -1$, see [11].

In a previous paper [31] the authors considered several aspects of the orientation preserving Hénon map (2), and also of the orientation reversing case, (8). The representations used for both maps were slightly different: the symmetry line was located in $y = 0$ instead of $y = -x$. One can obtain the representations used in [31] via the change of variables $(X, Y) = (x - y, x + y)/2$, and renaming (X, Y) as (x, y).

For reader's convenience we briefly recall some relevant facts for the orientation-preserving case, summarizing part of the results in [31]. This map will appear as a limit map modelling the dynamics of the main accelerator mode islands which cause the changes in the diffusive behaviour. For these purposes one needs to investigate the relative area of the accelerator modes and, also, the chaotic area confined inside the islands since trajectories within the confined chaotic region can be ejected to the chaotic sea by changing the relevant parameters. In this section we analyse these properties for the Hénon map.

2.1 Measure of the set of confined orbits

In Figure 1 we show the measure, $\mu(c)$, of the set of bounded orbits as a function of c for the map HP_c, as given in (2).

To produce Figure 1 we compute the maximal Lyapunov exponent, $\Lambda(p)$, for initial points p chosen in a narrow grid of points, and for many values of c. A typical spacing in the coordinates x and y for the grid is 0.0005. In most of the cases we first compute a transient of 10^6 iterates before starting to compute $\Lambda(p)$. In this way we detect most of the points which escape. A simple escaping criterion follows from the fact that if some forward iterate of p has x-component with $x < -1$, it will escape. A number of iterates $m = 10^6$ is also used to produce an estimate of $\Lambda(p)$. If the value obtained is below 2×10^{-5}, the orbit of p is considered to be regular and, hence, bounded. Otherwise it is considered to be chaotic. In the latter case, we continue with additional iterations (up to 10^8 and in some cases up to 10^{10}) to check if we can consider the chaos as confined or if the orbit of p is finally escaping.

The sudden decrease of $\mu(c)$ at some values of c corresponds to the destruction of the last invariant curves surrounding the islands. For example, near $c = 1$ we observe a sudden change in $\mu(c)$ which corresponds to the destruction of all the rotational invariant curves surrounding the period-4 islands.

The magnification shown in Figure 1, right, displays the self-similarity of $\mu(c)$ due to islands of a higher period. Such a Figure was first published in [17], and with higher precision in [28] for an equivalent version of the Hénon map given by Karney et al. in [17]. It appears as an approximation of the dynamics of the accelerator modes. This approach was refined in [31] and is summarized in Section 3. As an example, the large jump near $c = 0.91$ corresponds to the breakdown of invariant curves around the islands of rotation number $2/9$, while the jump shortly after $c = 0.96$ corresponds to the breakdown of invariant curves around the islands of rotation number $3/13$. It is not difficult to identify all the jumps shown in these plots.

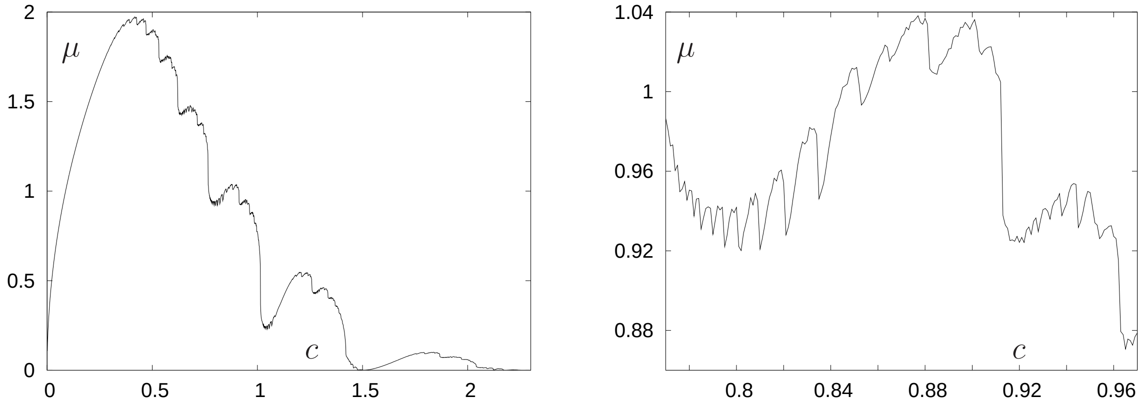

Figure 1: Left: measure $\mu(c)$ of HP_c of the set of confined points as a function of c. Right: a magnification in the range $c \in [0.77, 0.97]$ to provide evidence of the self-similar properties of $\mu(c)$.

The patterns shown in Figure 1 will show up again for some parameters of the standard map in next section. But similar patterns appear in more general systems, see [38]. In particular they appear in problems like the Michelson system [7] or in the Restricted Three-Body Problem [39].

2.2 Measure of the set of confined chaotic orbits

Among the points with bounded orbit there are, however, some which display chaotic behaviour. The Lyapunov exponent allows us to detect them. A natural question is, hence, how does the measure M of this set change with the value of c. This is shown in Figure 2 left. The plot shows quite a sharp change in its behaviour due to the infinitely many chains of islands in the system (which exist for any rotation number $\rho \in \mathbb{Q} \cap (0, 1/2]$). Each chain of islands has an associated hyperbolic periodic orbit, whose invariant manifolds generically split, generating some amount of chaos. It is confined until the invariant curves, that surround these chaotic orbits, break down. Even considering that the computations shown in Figure 2 have been done with a 10^{-3} step in c, a careful examination of the data allows us to detect several hundreds of peaks.

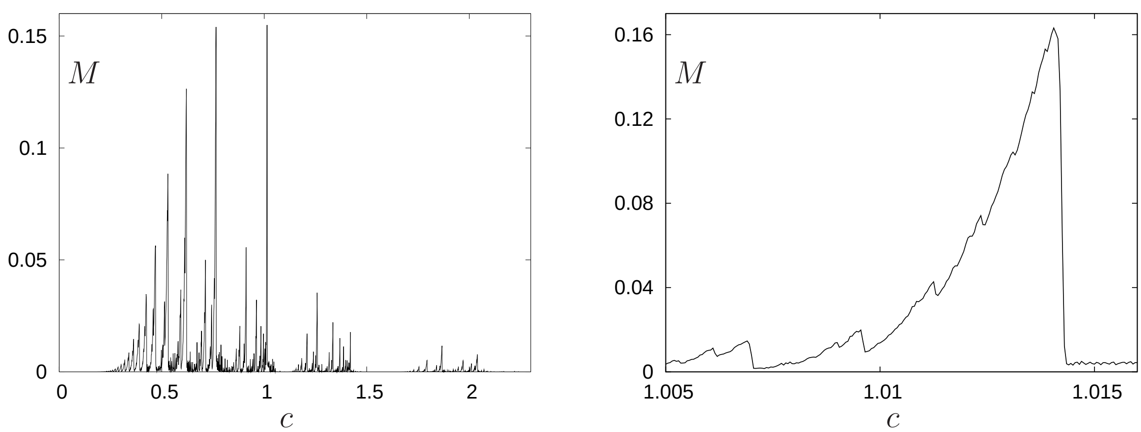

Figure 2: Left: Measure M of the set of confined points with chaotic dynamics as a function of c. Right: Magnification of the left plot to show what happens before and after the breakdown of the rotational invariant curves surrounding the period-4 island.

The magnification in Figure 2 right, computed with step 10^{-4} in c, shows what happens before the breakdown of the invariant curves around the islands of period 4. The confined chaotic region is created by the homoclinic tangle formed by the invariant manifolds of the period-4 hyperbolic orbit. This period-4 orbit is created at $c = c^0_{1/4} = 1$. The destruction of all the outermost invariant curves surrounding the islands of rotation number $\rho = 1/4$ takes place at $c = c_{1/4} \approx 1.0141$. Hence, for values of $c \gtrsim c_{1/4}$, the trajectories that were previously confined (i.e. those trajectories in the confined chaotic regions for $c \lesssim c_{1/4}$) diffuse. The different chains of small islands contained in the zone that was confined capture orbits for long times (stickiness) and change the global diffusion properties of the system.

3 The standard map for large parameter values

In this Section we consider Chirikov's standard map [1]:

$$M_k : \begin{pmatrix} x \\ y \end{pmatrix} \rightarrow \begin{pmatrix} \bar{x} \\ \bar{y} \end{pmatrix} = \begin{pmatrix} x + \bar{y} \\ y + k\sin(2\pi x) \end{pmatrix}, \tag{3}$$

defined on the unit torus $\mathbb{T}^2 = \mathbb{S}^1 \times \mathbb{S}^1$, and for large values of the parameter k. By large here we mean that most of the phase space is filled apparently by a chaotic sea, so for $k = \mathcal{O}(1)$, at least. But we shall be mainly interested also on the map defined in the cylinder $\mathbb{S}^1 \times \mathbb{R}^1$, to study the diffusion in the action variable. We shall denote then the standard map as $\bar{M}_k$, that is,

$$\bar{M}_k : \begin{pmatrix} x \\ y \end{pmatrix} \rightarrow \begin{pmatrix} \bar{x} \\ \bar{y} \end{pmatrix} = \begin{pmatrix} x + \bar{y} \ (\mathrm{mod}\ 1) \\ y + k\sin(2\pi x) \end{pmatrix}, \tag{4}$$

where no (mod 1) is taken for $\bar{y}$. For instance, for k integer, the point $(1/4, 0)$, which is fixed under M_k, jumps for k units under $\bar{M}_k$.

Here, for reader's convenience, the results of [31] on the existence, size and local dynamics of accelerator mode orbits for $\bar{M}_k$ are summarized. Numerics on the destruction of invariant curves around islands are also presented, with emphasis on the evolution, as the parameter increases, of the full set of such objects.

3.1 Measure of the set of regular points

For large enough values of k the map (3) has no rotational invariant curves. This has been proved for $2\pi k > 63/64$, see [23]. We also refer to [15] where it was proved for $k = 0.9718$. On the other hand, the so-called Grenee's threshold k_G [13] refers to the smallest value of k such that for $k > k_G$ the map (3) has no rotational invariant curves. There is strong numerical evidence that $2\pi k_G \approx 0.971635406\ldots$. See [33] for example, where a geometrical method based on the appearance of heteroclinic intersections preventing the existence of these curves, allows to obtain refined values for k_G. For increasing values of $k > k_G$, the phase space gets filled by a chaotic sea only showing small stability islands, though often there are none that are visible.

In [31] extensive numerics on the size of the regular area of the phase space were presented, showing that there are some special islands appearing periodically in k, and scaled in some sense. The existence of some of these islands (around $p_1^{1,2}$ and p_2 for M_k, given in Table 1) was already proved by Chirikov in [1]. In a fine grid on the phase space, let us denote as $A_r(k)$ the fraction of initial conditions for which we consider the maximal Lyapunov exponent to be zero, which depends on k (as we did in Section 2). In Figure 3 one can see the quantity $A_r(k)$, computed on a $(5 \times 10^{-5}) \times (5 \times 10^{-5})$ grid for values of k between 1 and 11. There seem to be some structures around integer and half-integer values of k, which appear repeated but scaled, both in area and range in k, when they exist. At a first glance,

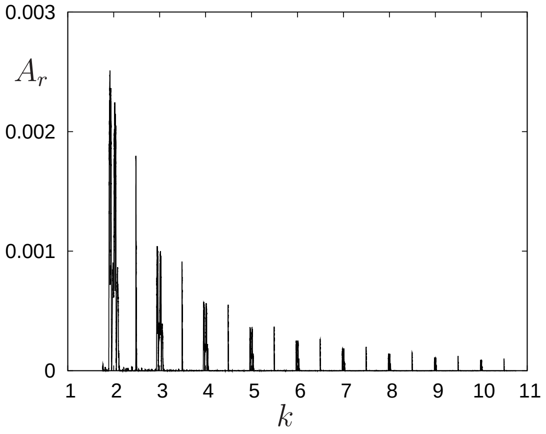

Figure 3: Relative measure $A_r(k)$ in the phase space of M_k of points whose maximal Lyapunov exponent can be considered to be zero, as a function of the parameter $k = 1.75(0.00005)10.75$. As usual the notation $k = \alpha(\beta)\gamma$ denotes values of k between α and γ with step β.

the area scales as $1/k^2$ ($1/k$ in both x and y variables) and the range in k scales as $1/k$. Other structures, not close to these values of k are very small.

Table 1 summarizes the orbits whose nearby dynamics produce the variation in the relative regular area $A_r(k)$ shown in Figure 3. These orbits appear near each integer n and half-integer n' values of k, and numerical continuation of them allows to conjecture for which values of the parameter they have an elliptic-hyperbolic and period-doubling bifurcations, which in turn depend on the integer or half-integer values to which the parameter k is close.

The orbits near integer values lying on $y = 0$ are the well-known accelerator mode orbits of $\bar{M}_k$ [35].

<table>
<tr><th></th><th>Position</th><th>Period</th><th>k-EH</th><th>k-PD</th></tr>
<tr><td rowspan="3">$n \in \mathbb{Z}$</td><td>$p_1^1 = (1/4, 0)$</td><td>1</td><td>$n \star$</td><td>$n + 2/(n\pi^2)$</td></tr>
<tr><td>$p_1^2 = (3/4, 0)$</td><td>1</td><td>$n \star$</td><td>$n + 2/(n\pi^2)$</td></tr>
<tr><td>$p_2 = (1/4, 1/2)$
$(3/4, 1/2)$</td><td>2</td><td>$n - 2/(n\pi^2)$</td><td>$n \star$</td></tr>
<tr><td>$n' \in \mathbb{Z} + 1/2$</td><td>$p_4 = (1/4, 1/2)$
$(1/4, 0)$
$(3/4, 1/2)$
$(3/4, 0)$</td><td>4</td><td>$n' - 1/(2n'\pi^2)$</td><td>$n' \star$</td></tr>
</table>

Table 1: Position, period and values of the parameter for which the orbits have elliptic-hyperbolic bifurcation (EH) and period-doubling bifurcation (PD). The inputs in the table labelled with $\star$ mean that it happens exactly at these particular values of k.

3.2 Some theoretical results on the main islands in the standard map

The numerics shown in Figure 3 and Table 1 suggests that these special orbits appear scaled at each integer and half-integer value of k. In [31] this fact was used to derive an expression of the limit dynamics around them. This is summarized in the following

Proposition 1. *There exists a limit behaviour of the dynamics around $p_1^{1,2}$ and p_2 (resp. p_4) under scalings in x, y and k by $1/n$ for $n \in \mathbb{Z}$ (resp. $n - 0.5 \in \mathbb{Z}$). Moreover, these limit maps are conjugated to area preserving orientation-preserving (resp.-reversing) Hénon maps, depending on a suitably scaled parameter.*

The proof of this result follows from considering suitable Taylor expansions in x, y and k of M_k around the orbits and values of the parameter in Table 1 labelled with $\star$, using suitable scalings for k near an integer (or half-integer) value n. Concretely, in the case of p_1^1 for period $\nu = 1$ in Table 1 we introduce new variables X, Y defined by $x = 1/4 + X/n, y = Y/n$ and a new parameter k' by $k = n + k'/n$. Expanding (3) we obtain a limit map L_1 (5) plus a remainder $\mathcal{R}$. In (5) we use again x, y instead of X, Y to denote the phase variables, while we keep the name of the new scaled parameter as k' to stress out that it measures the scaled distance to the nearest integer.

Taking into account that the confined points under (5) are contained in a compact set, the remainder $\mathcal{R}$ has a bound of the form $|\mathcal{R}| < \mathcal{B}/n^2$, where $\mathcal{B}$ depends on k'. This follows immediately from the Taylor expansions and of the alternating character of the series.

For a given value of k' we have estimated, numerically, the set of non-escaping points under L_1 using a fine grid. Given $n \in \mathbb{N}$ we compute $k = n + k'/n$, as said before. For each one of these points, the image under M_k (using the above mentioned scalings) has been computed and compared to the one given by L_1. The value $\mathcal{R}$ is taken as a measure of the error and multiplied by n^2 gives a bound for $\mathcal{B}$. It is checked that this bound is essentially independent of the value of n.

For values of k' such that the corresponding value of c (see Table 2) belongs to $[0, 1]$ (i.e., up to the value of c for which the 1:4 resonance appears) one can take $\mathcal{B} = 0.004$; for $c \in [1, 1.5]$ (i.e., up to the 1:3 resonance) one can take $\mathcal{B} = 0.02$, and up to $c = 2$ (period doubling) one can take $\mathcal{B} = 0.05$ (except, perhaps, at some tiny islands far away from the main confined domain). Higher bounds of $\mathcal{B}$ (up to 0.085) have to be taken at the end of the period doubling cascade. But this is quite irrelevant due to the tiny size of the islands.

The case of p_1^2 is identical to p_1^1 via a rotation of angle π around the point $(1/2, 0)$. For the case p_2 of period $\nu = 2$ one can introduce new variables X_1, Y_1 around $(1/4, 1/2)$ by $x = 1/4 + X_1/n, y = 1/2 + Y_1/n$ and X_2, Y_2 around $(3/4, 1/2)$ by $x = 3/4 - X_2/n, y = 1/2 - Y_2/n$. As before, we introduce k' by $k = n + k'/n$. Then the image of (X_1, Y_1) under M_k is expressed in the (X_2, Y_2) variables as given by (6) plus a remainder $\mathcal{R}$ and the same happens for the image of (X_2, Y_2) expressed in the (X_1, Y_1) variables. In (6) we also rename the phase space variables as x, y. The bounds of the remainder are identical to the ones in the $\nu = 1$ case.

For $\nu = 4$ let us denote as $p_4^{(j)}, j = 1, 2, 3, 4$, the points which appear in Table 1, in the order given there. It turns out that the passage from a vicinity of $p_4^{(1)}$ to a vicinity of $p_4^{(3)}$ under M_k^2 is described by the map given in (7) plus a remainder $\mathcal{R}$. The value of $|\mathcal{R}|$ is bounded, similar to the above cases, by $\mathcal{B}/(n')^2$, where n' is the closest element to k in $\mathbb{Z} + 1/2$. We assume $n' \geq 3/2$. The same expression is found for the passage from a vicinity of $p_4^{(3)}$ to a vicinity of $p_4^{(1)}$ under M_k^2.

To this end we introduce new variables (X_1, Y_1), (X_2, Y_2), (X_3, Y_3) around $p_4^{(1)}$, $p_4^{(2)}$, $p_4^{(3)}$, respectively, by $x = 1/4 + X_1/n' \, y = 1/2 + Y_1/n'$, then $x = 1/4 + X_2/n'$, $y = Y_2, /n'$ and, finally, $x = -1/4 - X_3/n'$, $y = 1/2 - Y_3/n'$. We also introduce a new parameter k' given by $k = n' + k'/n'$. The passage from (X_1, Y_1) to (X_3, Y_3) is the one given in (7), again using (x, y) for the variables, plus the remainder $\mathcal{R}$. In the range of interest of k', from the elliptic-hyperbolic bifurcation at $-1/(2\pi^2)$ till the end of the period-doubling cascade at ≈ 0.00778 one can take the bound $\mathcal{B} < 0.0251$.

Summarizing, one obtains the limit maps

$$L_1 \quad : \quad \begin{pmatrix} x \\ y \end{pmatrix} \mapsto \begin{pmatrix} \bar{x} \\ \bar{y} \end{pmatrix} = \begin{pmatrix} x + \bar{y} \\ y + k' - 2\pi^2 x^2 \end{pmatrix} \tag{5}$$

Map	Sym. line	Hénon map	New parameter	Scaling
L_1	$y = 0$	HP_c	$c = \pi\sqrt{2k'}$	$\sqrt{2}\pi/c$
L_2	$y = 2x$	HP_c	$c = \sqrt{4 + 2k'\pi^2}$	$\sqrt{2}\pi/c$
L_4	$y = 2x$	$(HR_c)^2$	$c = \sqrt{1 + 2k'\pi^2}$	$2\pi^2/c$

Table 2: Hénon maps to which L_ν, $\nu = 1, 2, 4$ are conjugated. The new parameter and scalings in x and y are given in the last two columns.

around p_1^1 and p_1^2,

$$L_2 : \begin{pmatrix} x \\ y \end{pmatrix} \mapsto \begin{pmatrix} \bar{x} \\ \bar{y} \end{pmatrix} = \begin{pmatrix} -x + \bar{y} \\ -y - k' + 2\pi^2 x^2 \end{pmatrix} \tag{6}$$

around p_2 and

$$L_4 : \begin{pmatrix} x \\ y \end{pmatrix} \mapsto \begin{pmatrix} \bar{x} \\ \bar{y} \end{pmatrix} = \begin{pmatrix} -x - y - s_0 + \bar{y} \\ -y - s_0 - s_1 \end{pmatrix} \tag{7}$$

around p_4, where $s_0 = k' - 2\pi^2 x^2$ and $s_1 = k' - 2\pi^2(x + y + s_0)^2$.

For the different limit maps L_ν, $\nu = 1, 2, 4$ one can explicitly find the changes of variables which relate them to area preserving Hénon maps HP_c for $\nu = 1, 2$ and HR_c (8) for $\nu = 4$. For the area preserving orientation reversing Hénon map we consider the following representation

$$HR_c : \begin{pmatrix} x \\ y \end{pmatrix} \to \begin{pmatrix} c(1 - x^2) + y \\ x \end{pmatrix}. \tag{8}$$

These changes of variables consist in performing a suitable rotation to match the symmetry lines of L_ν with the ones of the corresponding area preserving Hénon maps, some scalings in the x and y variables (with the same scaling factor in both variables) which include a reparametrisation.

In Table 2 one can find the original symmetry lines of each of the L_ν, the area preserving Hénon map to which they are conjugated to and the reparametrisation and the scaling factor of the x and y variables needed to relate them to Hénon maps. See Figure 4, right, for an example.

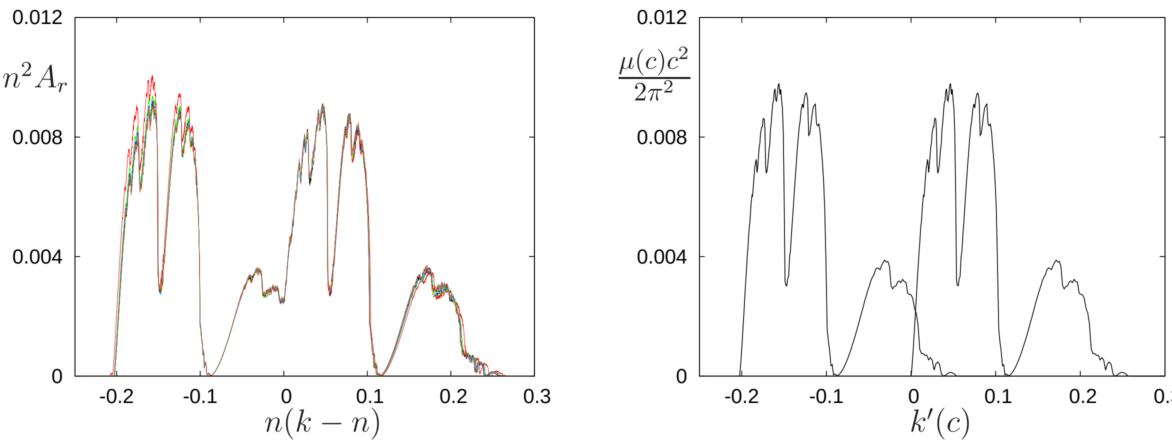

Figure 4: Comparison of the plot in Figure 3 with the evolution of the scaled areas obtained directly from the Hénon map (see Figure 1) via the changes available in Table 2. Left: Superimposed scaled areas $n^2 A_r(k)$ as a function of $n(k - n)$, for $n = 2, 3, \ldots, 10$. Right: Evolution of the regular area of the islands around the points $p_1^{1,2}$ and p_2 (see Table 1). Concretely, we plot $\mu(c)c^2/(2\pi^2)$ as a function of $k'(c)$, where $k'(c) = c^2/(2\pi^2)$ for $p_1^{1,2}$ and $k'(c) = (c^2 - 4)/(2\pi^2)$ for p_2.

This result allows us to recover the information of the scaled evolution of the regular areas directly from the evolution of the Hénon map in Figure 1, left. Hence, we can relate the local loss of the diffusive behaviour of $\bar{M}_k$, with the evolution of the phase space of Hénon maps.

The idea to derive a return map around the islands via Taylor expansions was already used by Karney et al. in [17], with a truncation to obtain the simplest nontrivial expression around the accelerator modes.

3.3 Numerical evidences on the size of the main islands

The scalings in Proposition 1 describe how the size of the main islands scales as k increases, and the order of the truncation error given in (5), (6) and (7) gives an idea of how the dynamics differs from an area preserving Hénon map.

Mainly, the islands responsible for the loss of diffusive behaviour of $\bar{M}_k$ are the accelerator mode orbits lying on $y = 0$ ($p_1^{1,2}$ in Table 1). In Figure 4 we show the data in Figure 3 around integer values of the parameter, where we have used the scalings by plotting $n^2 A_r(k)$ as a function of the scaled parameter $n(k-n)$ for $n = 2, 3, \ldots, 10$.

One can observe that, even though n is at most only of the order of 10 in Figure 3, the evolution of the islands is fairly well approximated by the evolution of the main stability islands of the Hénon maps obtained when we neglect the higher order terms in the limit expressions (5), (6) and (7).

3.4 On the destruction of rotational invariant curves

If our system depends on a parameter which measures the distance to integrability [41], a KAM approach tells us that for a prescribed invariant curve there has to be a balance between the twist condition, the Diophantine properties of the rotation number of the invariant curve and the size of the parameter, so that the sequence of iterations to obtain a conjugation between the dynamics of the invariant curve and a rigid rotation converges. The estimates on the maximal size of the parameter for fixed twist and Diophantine properties are far from practical, and a geometrical approach, such as the obstruction criterion [33] is more suitable for actual computations.

The effect of the presence of stability islands in the dynamics of orbits in a chaotic sea can not be always averaged out due to the stickiness effect, produced by the rich hierarchical island-around-island structure surrounding it, that is, the satellite islands and the invariant Aubry-Mather Cantor sets surrounding both the main island and the satellite islands (and the islands around satellite islands and so on). This structure can be very different for close values of the parameter, and as it evolves it can produce significant changes in the overall dynamics of our system.

In Figures 5 and 6 we show how the distribution of invariant curves around islands evolves as the parameter changes. As an example we have used the accelerator mode orbit which is in $(1/4, 0)$ for $k = 1$. We have estimated the values of the pairs (x, k) of x at the right hand side of the hyperbolic periodic point and of parameter k for which there are invariant curves. For the 1/4 hyperbolic periodic point in Figure 5 (see Figure 9 right for a sketch of the phase space near these parameter values) and for the 3/13 and 2/9 hyperbolic periodic points in Figure 6. In the last case the points are taken to the left of the corresponding periodic hyperbolic point.

We have proceeded as follows: for a fixed value of k, we consider a grid of points with spacing 10^{-6} on the $y = 0$ line. For each of these points, we have computed an approximation

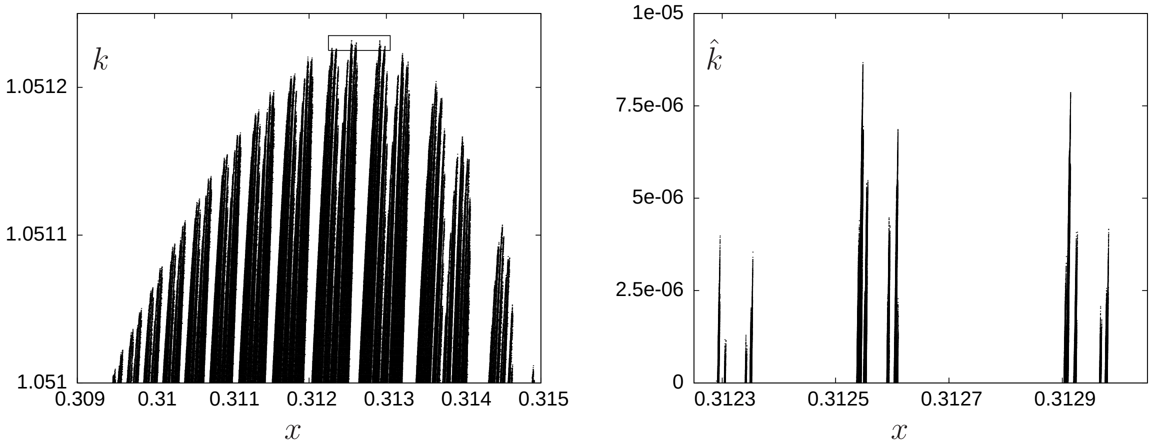

Figure 5: Initial conditions in the (x, k) plane taken on $y = 0$ for which there exist rotational invariant curves surrounding the accelerator mode island. The right plot is a magnification of the box in the left plot. Computations for values of the parameter after the 1/4 resonance. The parameter $\hat{k}$ in the right plot is related to k by $\hat{k} = k - 1.051225$.

of the Lyapunov exponent. If considered zero, it was a candidate to invariant curve so its rotation number was approximated via the method explained in the appendix of [36]. If it could be considered irrational, we plotted this pair (x, k).

In these figures we observe black bands emanating from the horizontal axis. The white strips in these bands correspond to islands which are perfectly identifiable. In the black bands, one can see "tongues" which, when zooming, reach the x axis: they correspond to instability zones produced by the splitting of the separatrices of hyperbolic periodic points.

For $k = 1.051$, at the bottom of Figure 5 one can observe relatively large gaps in the Cantor structure of invariant curves. They correspond to the existence of islands. The rightmost gap, for $x \in [0.314050, 0.314312]$, corresponds to a rotation number $\rho = 10/41$, while the leftmost one, for $x \in [0.309577, 0.309634]$, corresponds to $\rho = 30/121$. The rotation numbers of the islands in the largest gaps are of the form $2j/(8j + 1), j = 5, \ldots, 15$. Due to the symmetry properties of M_k, islands with ρ of the form p/q with p even appear to the right of the fixed point, while if p is odd they appear to the left.

Furthermore, to the right of the displayed domain for $k = 1.051$ an island with $\rho = 8/33$ appears for $x \in [0.315087, 0.315453]$ and one to the left, with $\rho = 32/129$, is found for $x \in [0.309386, 0.309443]$.

It is also easy to identify some periodic hyperbolic points, which are at the birth of the destruction of nearby invariant curves. For instance, for the approximate values $x =$ 0.309508, 0.313708 and 0.314701 periodic orbits with $\rho = 31/125$, 11/45 and 9/37, respectively, are found.

For each elliptic periodic point, one can see that there are 2 invariant curves, one to the right and one to the left, surrounding a chain of islands. They both have similar rotation number, but their destruction is not simultaneous. In particular, the continued fraction expansion of the rotation numbers of the two highest tips which are shown in the magnification of Figure 5 are

$$[4, 14, 1, 1, 1, 1, 1, \ldots] \text{ and } [4, 13, 1, 1, 1, 1, 1, \ldots],$$

for the tips located near $x = 0.3125$ and $x = 0.3129$ respectively.

Finally, we note the quadratic shape of the envelope of the red points in the Figures 5 and 6. This can be explained as follows. To study the dynamics in the chaotic zone between the 1/4-periodic island surrounding the accelerator mode island and the last invariant curve (if exists) one can use a separatrix map model, see [1, 41]. At some (fixed) distance y_0 from

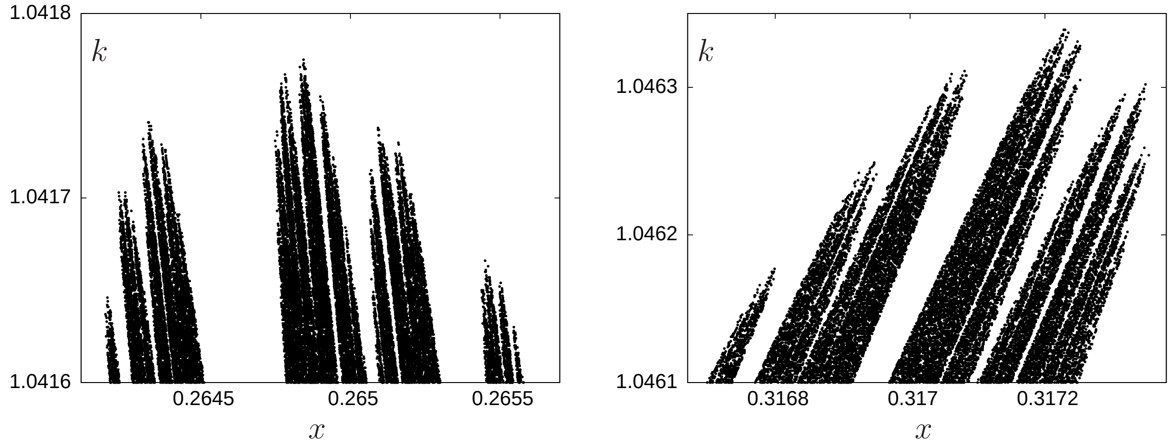

Figure 6: Initial conditions in the (x, k) plane taken on $y = 0$ for which there exist a rotational invariant curve with respect to the accelerator mode. Computations for values of the parameter after the: Left: 2/9 resonance. Right: 3/13 resonance.

the separatrices bounding the 1/4 islands, the separatrix map can be approximated by a standard map $\bar{M}_k$ with $k \sim 1/|y_0|$. This explains why the boundary of the black points in Figures 5 and 6 resembles the critical function of the standard map M_k. We recall that the critical function (also referred as fractal diagram) relates the frequency ω with the value of $k = k(\omega)$ for which the invariant curve with frequency ω breaks down. In our plots we represent x instead of ω as the x-coordinate, but there is a one-to-one correspondence guaranteed by the non-vanishing twist property. The breakdown of invariant curves can be investigated using a renormalization scheme approach, see [24]. The renormalization scheme implies that the locally most robust invariant curves correspond to noble rotation numbers. Hence the maxima observed in the figures are related to noble numbers, as was noticed above for the two highest tips. Moreover, for the golden rotation number g the corresponding renormalization operator implies that the distance $\Delta\omega$ to the nearby noble numbers scales as

$$\Delta k \sim -|\Delta\omega|^{\eta},$$

where $\eta = |\log(\delta)/(2\log(g))| \approx 0.5063$, see [24]. Here δ refers to the inverse of the convergence ratio of the renormalization scheme, see (13) in Section 6.4. See also related comments in [25]. Moreover, a similar behaviour is expected for any noble number. This implies that each of the tips shown is expected to have (locally) a quadratic shape again. We remark that the renormalization process gives local information around the most robust noble in a given interval. Nevertheless, in the figures one observes that the quadratic shape has a more global character (although the considered range of x relatively small).

4 Elementary approaches to the diffusion properties

We start here with simple approaches to the diffusion properties of the $\bar{M}_k$ as given in (4) for large k. In fact these approaches provide a good idea of the diffusion for most of the values of the parameters if they are sufficiently large. Then we shall compare with a better measure of the properties of the dynamics. Concrete details and explanations will be given in the next sections.

We consider here the diffusion in the y variable for $\bar{M}_k$. The main conclusion will be that there are ranges of the parameter where the behaviour is not of diffusive type, even starting in the chaotic domain. But the width of these ranges tends to zero as $k \to \infty$.

4.1 The quasi-linear approximation

For large k the statistical description of the dynamics in the chaotic zone, assuming that the measure of the regular zone is negligible in front of the one of the chaotic zone, can be done via the simplest (homogeneous) diffusion equation [2]

$$\frac{\partial f}{\partial t} = \frac{1}{2} D(k) \frac{\partial^2 f}{\partial y^2},$$

where $f = f(y,t)$ is the density of points, t denotes the number of iterations and y is the momentum. The transition density of a Brownian motion starting at 0 with variance $\sigma^2 = 1$ satisfies the previous heat equation, that is, the infinitesimal generator of the underlying Feller process is $\frac{1}{2}\frac{\partial^2 f}{\partial y^2}$. Note that this approach assumes that the effect of the angles x averages properly, and then the diffusion equation describes the dynamics in the y direction. An improvement to take into account the influence of x will be given in Section 4.2.

Let us denote as $(x_j, y_j) = \bar{M}_k^j(x_0, y_0)$ the values of the successive iterates of a point $(x_0, y_0) \in \mathbb{S}^1 \times \mathbb{R}^1$. Let $\Delta^j y = y_j - y_0$ be the difference in actions after j iterates. The average diffusion rate for $\bar{M}_k$, $D(k)$, can be evaluated as the limit

$$D(k) = \lim_{n\to\infty} \frac{\langle (\Delta^n y)^2 \rangle}{n}. \tag{9}$$

where $\langle \cdot \rangle$ stands for the ensemble average. Note that in this definition the mean $\langle (\Delta^n y) \rangle$ is assumed to be zero, so it is not included in (9). Despite this fact holds true in our setting, when we compute $D(k)$ or some variant of it, to obtain the variance we include that missing term: $\sigma^2 = \langle (\Delta^n y)^2 \rangle - \langle (\Delta^n y) \rangle^2$.

Under the assumption that we can average out the effect of the angles in $\bar{M}_k$, and no accelerator modes show up in the phase space, $D(k)$ takes the value

$$D_{ql}(k) = \frac{k^2}{2}, \tag{10}$$

which is usually referred to as the quasi-linear value. If we normalize (10), to skip the effect of k, one should obtain the value $D_{ql,n} = 1/2$.

4.1.1 Selecting initial points

An important point, for this section and next one, is the selection of initial points to be iterated under $\bar{M}_k$, to measure the diffusion properties. We want to make sure that these points are taken on the "chaotic sea", i.e., outside any island. To this end we have used the following method to select initial points:

a) Compute an approximation of the unstable manifold $W^u_{k,p}$ of some periodic hyperbolic orbit of period p. This can be done in an efficient way via the parametrisation method (see [37]) at some high order (typically between 20 and 50). Except in the case $p = 1$ (i.e., for the hyperbolic fixed point) one has to compute first the Taylor expansion of M_k^p around the chosen point.

b) Let z be a parameter of the manifold and $g(z)$ the corresponding point in $W^u_{k,p}$. The invariance condition reads $M_k^p(g(z)) = g(\lambda z)$, where λ is the dominant eigenvalue at the chosen point and z has been normalized so that the linear term in $g(z)$ has modulus 1. Select a fundamental domain in $U = [z_0/\lambda, z_0]$ in which the invariance condition is satisfied with a prescribed tolerance (typically 10^{-20}).

c) Choose points in U, e.g. with uniform step in log scale, and iterate them n_0 times under M_k as a transient. These will be the selected initial points.

4.1.2 Results and interpretation

An idea on the goodness of the quasilinear approximation $D_{ql,n}(k)$ can be obtained by computing the first term $\langle(\Delta^1 y)^2\rangle$ in the limit (9) via the method just described. We have used $p = 1$ in subsection 4.1.1 a), $N = 250,000$ points in U and have done $T = 10^6$ iterates. Note that, since we recorded $\Delta^1 y$ and $(\Delta^1 y)^2$ at each iterate, assuming uncorrelation, it is equivalent to take just one initial point and iterating it $T = 2.5 \times 10^{11}$ times or to consider $N = 2.5 \times 10^{11}$ initial conditions and doing just one iteration.

We have considered the values of the parameter $k = 0.72(0.001)6.1$, for which the phase space is filled with what seems to be a chaotic sea, except for the islands appearing near integer and half-integer values of the parameter studied in Section 3. After skipping the effect of k, the obtained approximation $\tilde{D}_{ql,n}(k)$ of $D_{ql,n}(k)$ differs from $1/2$ by less than 2×10^{-6} for most values of k.

However, there are parameters for which the computed value $\tilde{D}_{ql,n}(k)$ differs in a significative way from $1/2$ and it is below the expected value. The parameters k for which this occurs are seen to coincide with the ones for which islands are detected for M_k, as described in Section 3.3.

In Figure 7 we display the values of $1/2 - \tilde{D}_{ql,n}(k)$ as a function of k in the range mentioned above. Compare the left plot with Figure 3 in Section 3.3. Further details can be seen on the right plot, with $k \in [1.87, 2.13]$. No differences have been observed if we replace the unstable manifold of the fixed point by unstable manifolds of other periodic hyperbolic orbits to select the initial conditions.

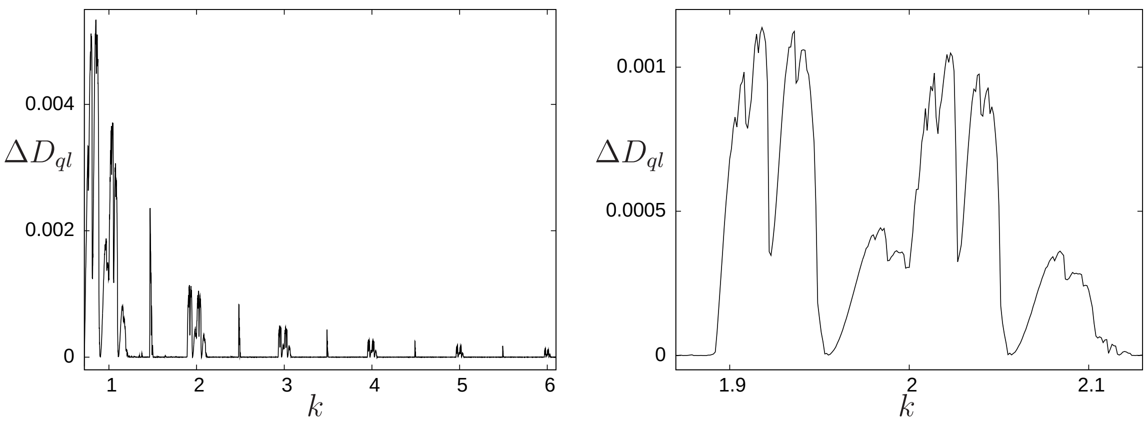

Figure 7: Values of $\Delta D_{ql} = 1/2 - \tilde{D}_{ql,n}(k)$, where $\tilde{D}_{ql,n}(k)$ is the numerically estimated average one step diffusion rate, as a function of k. Left: results for $k \in [0.72, 6.1]$. Right: a magnification for $k \in [1.87, 2.13]$.

There is an easy interpretation to the results. The places where some islands are located, according to Section 3.3, are close to $x = 1/4$ and $x = 3/4$. The iterates of points in the chaotic zone can not enter into them. Hence, as in these domains the value of $(\Delta y)^2$ is, approximately, equal to k^2 and close to maximal, the contribution to the average is missing. This produces a decrease in the value of $\tilde{D}_{ql,n}(k)$ roughly proportional to the size of the island.

Note that this first term in the limit (9) is significatively different form all other terms. When one considers more than one single iterate, the value of $\langle(\Delta^n y)^2\rangle$ can not be easily averaged since functions like $k \sin(2\pi(x + y + k \sin(2\pi(x + \cdots))))$ appear. This kind of expressions are typically expanded in k by sums of Bessel functions as will be seen in the next Section, producing larger oscillations, as noted in [2].

4.2 A first improvement

A first improvement with respect to the quasi-linear approximation consists in taking into account the effects of the correlations between successive iterates. A nice description can be found in [19] and references therein. These effects can be studied using Fourier techniques. A simple correction factor, adapted to the notation and normalizations we use in this work, follows from formula (5.5.21) in [19] and the comments that follow after that formula. See also [29] and [42].

Hence, we should expect a corrected value for the normalized average diffusion rate given by

$$D_{cc}(k) = \frac{1}{2}\left[1 - J_2(2\pi k) + (J_2(2\pi k))^2\right], \tag{11}$$

where D_{cc} stand for "correlation corrected" and J_2 denotes the second Bessel function. The values of $D_{cc}(k) - 1/2$ tend to 0 as $k^{-1/2}$ when $k \to \infty$ with sinusoidal oscillations around 0.

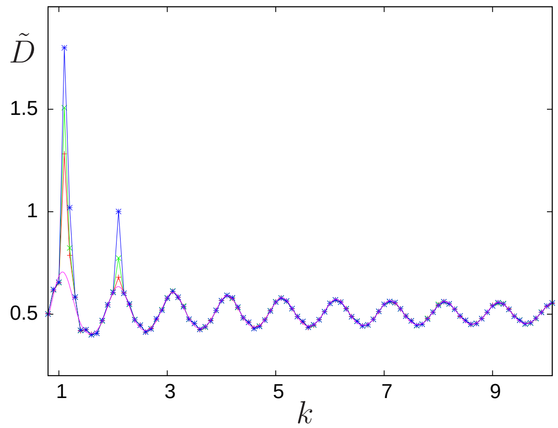

Figure 8: For a range of values of k, as horizontal variable, and using a large step in k, we show the values of the estimated diffusive properties of $\bar{M}_k$, after $10^3, 10^4$ and 10^5 iterates (in red, green and blue, respectively), for a sample of 10^5 initial conditions. The magenta curve shows the values of $D_{cc}(k)$ as given by (11). Here $\tilde{D}$ simply denotes the values for the different number of iterates including the normalization mentioned at the end of subsection 4.1.

In Section 5 we provide a method to estimate the true diffusive properties of $\bar{M}_k$. We shall see that the results depend on the number of iterates, T, after the transient. Explanations for these results will be provided in Section 6. For the moment being we display, in Figure 8, the comparison between the results using a sample of 10^5 initial conditions and values of T equal to $10^3, 10^4$ and 10^5 (in red, green and blue, respectively) and the ones using (11) (in magenta). Even taking into account that we have used the values of $k = 0.8(0.1)10.1$, one can observe big differences, mainly near 1 and 2. In fact, these differences appear shortly after every integer value of k in domains which become narrower as $1/k$ when k increases. Outside these domains, to be discussed in next section, the approximation provided by (11) is quite good. The two peaks seen in Figure 8 are just a preliminary indication of the richness that in subsection 5.2 will be shown to exist. This is one of the main motivations of this work.

5 Numerical evidences on the real diffusion properties

To have a correct estimate of the diffusive properties of $\bar{M}_k$ we should take into account how the "diffusion" depends on time, that is, on the number of iterates T and check that it is essentially independent on the size of the sample N, i.e. the number of initial points which are iterated under the map.

It is well-known that in a diffusive process, with constant diffusion coefficient, a sample of N points starting at a give value of y (or nearby values) after T iterates has a standard deviation σ_T which behaves as $\sqrt{T}$. Hence, when dividing σ_T by $\sqrt{T}$ it should tend to a constant, the diffusion coefficient, when T increases and, to minimize the effect of N, when the size of the sample also increases.

Consider a given initial value of y, say y_0 after the transient and reducing it to $\mathbb{T}^2$, that is $0 \leq y_0 \leq 1$ (or, equivalently, $-1/2 \leq y_0 \leq 1/2$). Let y_T the value after T iterates, without any further reduction to $\mathbb{T}^2$, that is, using $\bar{M}_k$. The standard deviation can be measured for the "jump" in y: $\Delta^T y = y_T - y_0$.

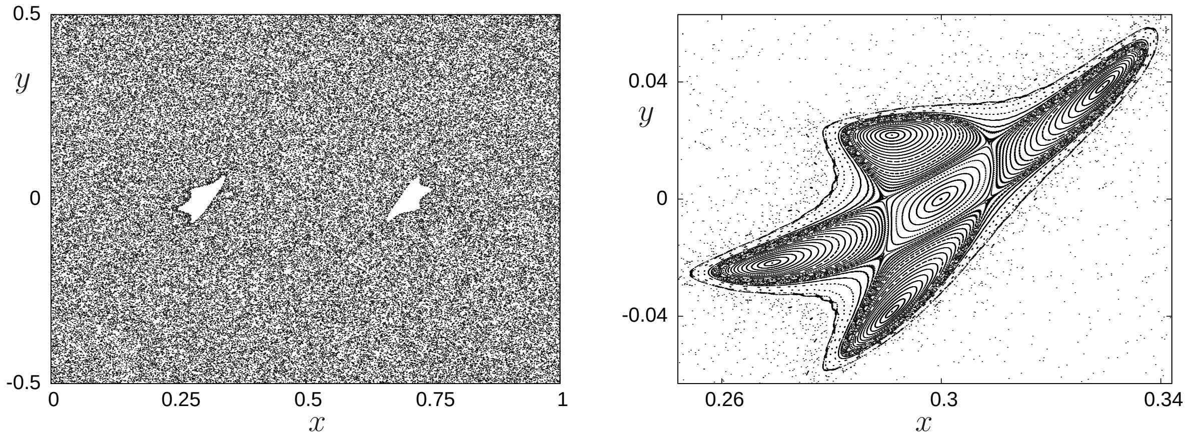

Figure 9: For $k = 1.05123$ the left plot shows an orbit of an initial point in the chaotic zone, reducing y to the range $[-1/2, 1/2)$. Two domains, around fixed points of M_k, are seen to be non accessible. The right plot shows details on the dynamics around the fixed points on the "left" island.

A typical orbit of a point in the chaotic zone is shown, reducing it to $\mathbb{T}^2$, in Figure 9 left. We see that it avoids a couple of islands located, approximately, around $(0.3, 0)$ and $(0.8, 0)$, where there are fixed points of M_k. The value used for the figure is $k = 1.05123$ and reasons for that choice of k will be given later. Compare also with the results shown in Figure 5. The right plot in Figure 9 shows a detail on the dynamics near the left fixed point. As points near the fixed point jump up by an amount close to one unit under iteration by $\bar{M}_k$, we call it "the positive island". In a similar way, the island on the right side of Figure 9 left will be denoted "the negative island". Accordingly, the fixed points inside these islands will be denoted as E_+ and E_-, respectively. Around the fixed point one can see several KAM curves, then a hyperbolic periodic orbit of period 4, the related islands of period 4 and, as given by the evidence in Figure 5 there are still invariant curves around these period-4 islands.

According to Figure 5 right, these curves persist until a value of k located in the range $(1.05123, 1.05124)$. Hence, the iterates of initial points in the chaotic domain can not enter inside the islands, because of the existence of these invariant curves.

The reason why we have selected values of k near the destruction of the invariant curves around the period-4 islands, as it can be seen in the details shown in Figure 13, relies on the measure of the confined chaotic domains for the Hénon map, see Figure 2 right. For period 4 it turns out that this measure is one of the largest ones. See more details in Figure 5 in [31]. However, a detailed inspection of the diffusive properties shortly after the destruction of the last invariant curve around islands with other rotation numbers (like 1/5, 1/6, 1/7,...,2/9, 2/11, ...,3/13,...) shows the same properties that will be described for rotation number 1/4. But to go deeply into some of the details of the phenomena for these rotation numbers the number of iterations has to be increased.

The results of the computations of $\sigma_T/\sqrt{T}$ show a strong dependence in T when period-1 islands exist, independently of the size of N if this one is large enough to provide a good estimate of σ_T. The methods used (some of them to be used also in Section 6.2) and which kind of data are recorded, are presented in Section 5.1, with results shown in Section 5.2.

5.1 Methods

As mentioned in Section 4.1.1 we have used initial data in $\mathbb{T}^2$ after a transient of $n_0 = 10^3$ starting in a fundamental domain of the unstable manifold $W^u_{k,1}$. Most of the results have been checked using also starting points in $W^u_{k,2}$, having an excellent agreement.

After the transient every initial point is iterated T times. The current values of y_T for different values of T (typically for powers of 2) are stored. At the end of the computation, for each selected value of k and each value of T, one has the standard deviation of a sample of N initial points, which is scaled by the current value of $\sqrt{T}$ and also by k to obtain a normalized value, as described in Section 4.1. Concretely, if a value $\sigma_T(k)$ has been obtained as standard deviation, we record the value

$$\sigma_{T,k} = \sigma_T(k)/(k\sqrt{2T}), \qquad \sigma_T^2(k) = \left\langle(\Delta^T y)^2\right\rangle - \left\langle(\Delta^T y)\right\rangle^2 \tag{12}$$

The additional $\sqrt{2}$ has been introduced to allow for comparisons with the normalized quasi-linear value $D_{ql,n}$.

It has been checked that the iterates of initial points can remain close to the islands for many iterations. Suitable explanations are given in Section 6.

One of the quantitative questions to decide is how to give a concrete meaning to the sentence “to remain close to the islands”. This has been used for the computations whose results are shown in Figure 13, i.e., for a very narrow range of values of k. Looking at Figure 9 right we decide to consider as “close to the islands” points which pass at a distance less than some amount r_b (fixed as 0.0775 for the data shown in Figure 13) from either E_+ or E_-. But it is clear that there are points clearly in the chaotic zone that enter this domain. Hence, to consider that the orbit of a point passes close to, say, the positive island, we require to be at a distance less than r_b from E_+ for, at least n_b consecutive iterates. As suitable value for n_b we have taken 2^7. The set of points where these two conditions are satisfied (proximity and permanence) will be denoted as “the vicinity of the island” and represented as $\mathcal{W}_{E_+}$ or $\mathcal{W}_{E_-}$.

This will allow us to have average estimates on the “trips” of the different initial points, that is, how many iterates they spend in the chaotic domain, how many close to the positive or negative islands, the probability to pass from the chaotic domain to $\mathcal{W}_{E_+} \cup \mathcal{W}_{E_-}$ and the mean time spent in these vicinities. All these data will be useful to understand the global dynamics, as described in Section 6.

Note that after the transient of 10^3 iterates it can happen that some point is already in $\mathcal{W}_{E_+}$ or in $\mathcal{W}_{E_-}$. This really do happens but the fraction of points in each one of these vicinities is below 1.5%.

5.2 Results

Figure 10 shows the results for $\sigma_{T,k}$ for $T = 2^{18}$, a sample size $N = 250,000$ and $k = 0.8(0.001)$ 10.1. Beyond the oscillations around 0.5, already observed in Figure 8, sufficiently well modelled by the values in (11), we see some wild behavior with several large peaks shortly after integer values of k. The size of the peaks and also the width of the ranges where this occurs behave, approximately, like $1/k$. A similar type of results can be found in [42].

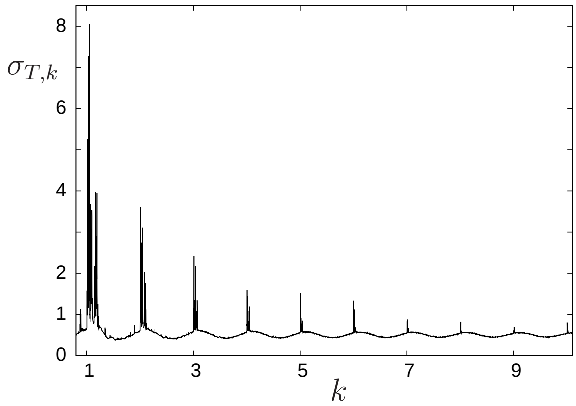

Figure 10: For $k = 0.8(0.001)10.1$ as horizontal variable, we represent the values of the estimates of $\sigma_{T,k}$, as vertical variable. See the text for the values of T and N.

Note that the ranges correspond to part of the places where M_k has fixed points (in $\mathbb{T}^2$), but not to the ranges where period-2, period-4 and several other periodic islands are found. The reason for this different behavior is elementary and will be given in Section 6.

In Figure 11 we show a detailed view of the previous result shortly after $k = 1$ and $k = 4$. Similar results have been obtained for many other ranges of k following integer values. The corresponding values have been obtained using $N = 10^6$ and for $T = 2^j, j = 16, 18, 20$ are displayed in different colors. The values of $\sigma_{T,k}$ increase with T.

Both parts of Figure 11 are quite similar, except by the different scaling in both the horizontal and vertical variables and minor details. The peaks are almost gone for k near 1.06 in the left plot and for k near 4.015 in the right one. For these values the elliptic fixed points of M_k have rotation number close to 1/3. According to the study of the standard map islands, and based on the properties of the Hénon map presented in Section 2, the islands around E_+ have a negligible size.

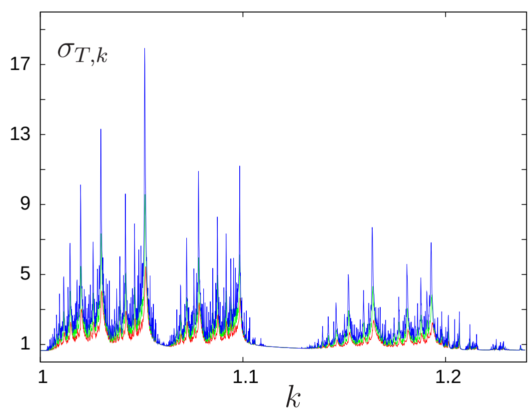

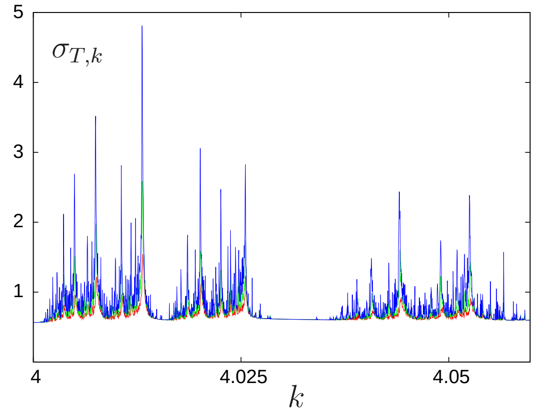

Figure 11: Details on the behavior of $\sigma_{T,k}$ near $k = 1$ (left) and $k = 4$ (right) for three increasing values of T. The concrete ranges of k are 1(0.0001)1.24 and 4(0.00003)4.06. See the text for the values of N and the different values of T used in the computations.

In Figure 12 we restrict our attention to the k intervals $[1, 1.06]$ and $[4, 4.015]$. As expected, both plots are quite similar. The values of N and the steps in k are the same as before, but the values used for T are now $2^j, j = 18, 20, 22$. Comparing with the parts of Figure 11 corresponding to the same intervals, we realize that the peaks have, roughly, the double value when T increases by a factor 4.

Each one of the peaks seen in Figure 12 occurs shortly after the breakdown of all the outermost invariant curves surrounding the islands around E_+ and E_- with a given rotation

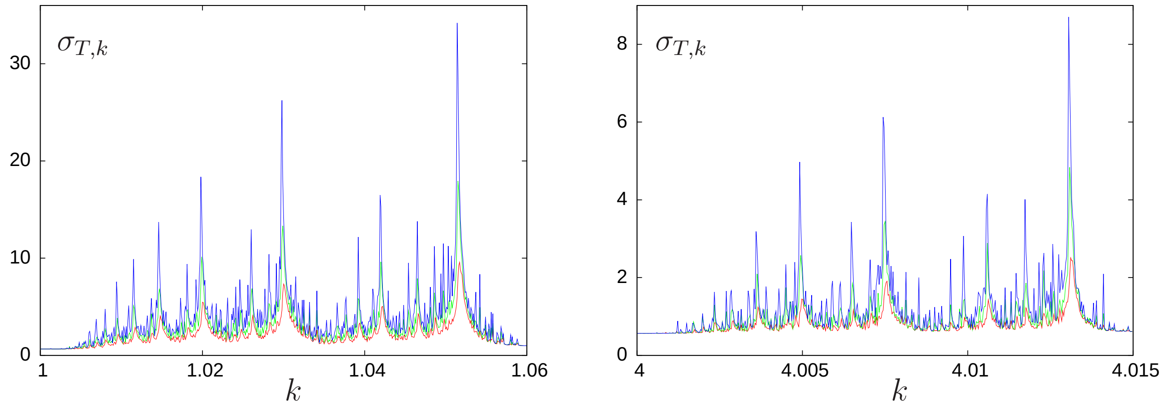

Figure 12: Further details on $\sigma_{T,k}$ in narrower ranges near $k=1$ (left) and $k=4$ (right). The values used for T have been increased by a factor 4 with respect to Figure 11.

number, ρ, which occurs for a critical value to be denoted as $k_{c,\rho}$. Approximate values of the location of the peaks in that figure and the corresponding rotation numbers are given in Table 3.

$10^4(k-1)$	514	465	419	392	298	260	198	146	115	94	80	69	61
ρ	1/4	3/13	2/9	3/14	1/5	2/11	1/6	1/7	1/8	1/9	1/10	1/11	1/12

Table 3: A sample of the values of k for which large peaks appear in Figure 12. For each value of k we give the rotation number of the islands such that the outermost invariant curve surrounding them has been destroyed for a nearby, smaller, value of k.

From now on we concentrate on the vicinity of the largest peak in Figure 12 using a large number of iterates. That is, for k around $k_{c,1/4}$. A similar behavior has been observed for other major peaks. It is apparent that the peak that we consider is the largest one for all $k>1$.

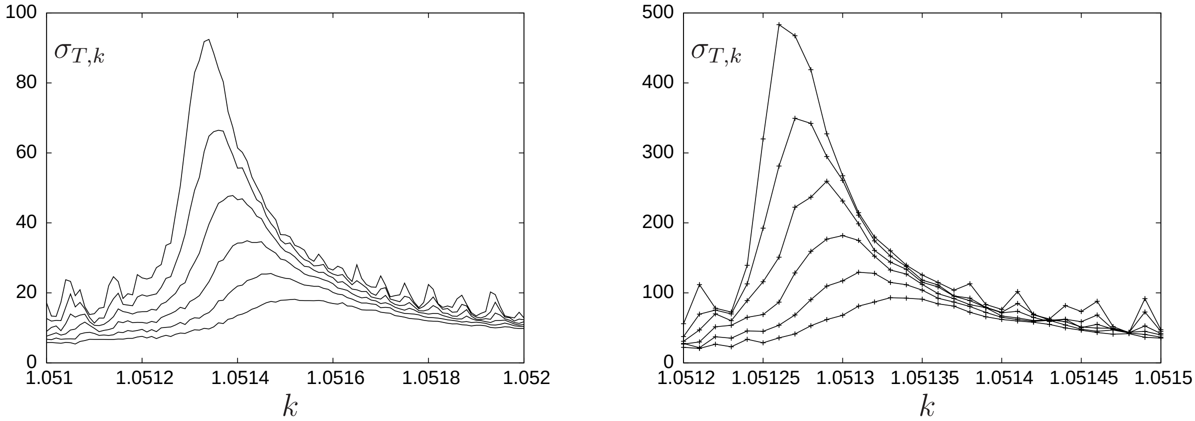

Figure 13: A sample of results near the largest peak in Figure 12 for large values of T. In the left plot the values of T go up to 2^{25} and in the right one they reach 2^{30}. See the text for additional details.

In Figure 13 the results in narrow domains around $k=1.0514$ are shown. In the left plot the number of initial points is $N=10^6$ while the values of $\sigma_{T,k}$ are shown for $T=2^j, j=20(1)25$. We have used $k=1.051(10^{-5})1.052$. In the right plot one has used $N=10^5$ and the values of $T=2^j, j=25(1)30$. The step in k is the same as in the left plot, but the range is reduced to $[1.0512, 1.0515]$.

The upper curve in the left plot, which reaches a value slightly larger than 92, can be identified with the lower one that can be seen in the right plot. The upper one in the right plot reaches a value slightly larger than 483. The ratio of these values is 5.25, a little bit below the square root of the ratio of the number of iterates ($T = 2^{30}$ on the right, $T = 2^{25}$ on the left).

We can summarize the observed results near a peak of $\sigma_{T,k}$ related to the breakdown of the invariant curves around an island of rotation number ρ as follows:

1. The maximal value of $\sigma_{T,k}$, for a given T, occurs for values of $k = k(T)$, the function $k(T)$ is decreasing and tending to $k_{c,\rho}$ as $T \to \infty$.

2. The values of $\sigma_{T,k(T)}$ tend to scale as $\sqrt{T}$. That is, the non-scaled standard deviation $\sigma_T(k)$, see (12), reaches a linear dependence in T, at least selecting the values of k in a way which depends on T. This implies that the dynamics in y is not Gaussian and the diffusion coefficient diverges. Otherwise, $\sigma_{T,k}$ would have finite limit. This is related to the fact that the escape time distribution from the stickiness region around the accelerator modes has infinite variance, see related comments in Section 6.3. At the end of Section 6.2 we return to this key point, and in Section 6.4 we will give a theoretical justification of it.

Note also that for large T the effect of little islands starts to be seen, see Figure 13.

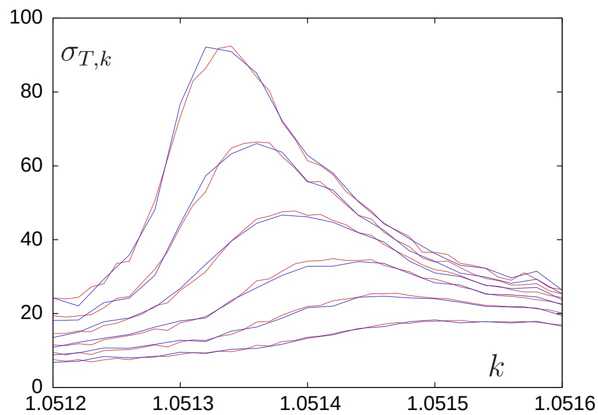

Figure 14: Comparison of the results for $T = 2^m, m = 20(1)25$ and a reduced set of values of k using double precision (in red, part of Figure 13, with a sample of 10^6 points) and quadruple precision (in blue, with a sample of 2×10^5 points).

To check the role of the arithmetics on the computations we have reproduced, using quadruple precision, the results in a subinterval of Figure 13 left. Concretely, we have taken a reduced set of values of the parameter $k = 1.0512(2 \times 10^{-5})1.0516$, a number of iterations of the form $T = 2^m$, $m = 20(1)25$ and a smaller size of the sample, $N = 2 \times 10^5$. The results, displayed in Figure 14, show a good agreement with the ones that have been produced with double precision.

6 Qualitative and quantitative approaches to the interpretation of the numerical results

In this section we first comment on the role that different invariant objects have on the statistical properties. Then we provide additional numerical information, mainly extracted from the computations leading to Figure 13. To compare with this information we include a study of the breakdown of the last rotational invariant curve (the one with golden rotation number) at the Greene's critical value of the parameter. After a presentation of some theoretical limit renormalization results, we are in condition to explain the shapes seen in the previous figures, concerning the behavior of the standard deviation as a function of T and N.

6.1 The role of different objects and phenomena

i) The accelerator modes.

For k integer the fixed point E_+ of M_k, located at $(1/4, 0)$, jumps k units up under $\bar{M}_k$. Despite starting at the chaotic sea, when entering $\mathcal{W}_{E_+}$ the orbit can mimic the behavior of E_+ for many iterates. Going away from $y = 0$ it will produce a major contribution to the standard deviation. The same is true for points entering $\mathcal{W}_{E_-}$, or even if an orbit visits $\mathcal{W}_{E_+}$ for a while, then it visits $\mathcal{W}_{E_-}$ (or, perhaps, $\mathcal{W}_{E_+}$ again) and successive visits to both domains are produced.

The situation is different when an orbit approaches the islands of period 2 or 4 (or higher periods). After visiting the vicinity of an island going up, the orbit visits the vicinity of one island going down in next iterate, having close to zero average (after 2 or 4) iterations. This explains the qualitative differences between Figures 3 and 10.

ii) The Cantor sets.

Consider, first, $k \leq k_{c,1/4}$, that is a value such that there still exist invariant curves around the period-4 islands. Orbits in the chaotic sea can not cross these curves to become trapped by the island. But when they have a breakdown, they are replaced by Cantor sets, the iterates can penetrate inside the domain that was bounded by the previous invariant curves, approach the period-4 islands, spend some time near tiny islands, etc, and, eventually, leave the domain through the gaps of the cantorus.

If $k > k_{c,1/4}$ the size of the gaps increases with the difference $k - k_{c,1/4}$. It becomes easier "to enter", but also the residence time in that domain decreases. This phenomenon is repeated at different scales around all the tiny islands visited by the iterates.

The effects can be seen on the "bumps" presented in Figure 15 and, in a cleaner way, in Figure 16.

iii) The stickiness.

In fact we should consider not just the breakdown of the last invariant curve around the period-4 islands. For $k \leq k_{c,1/4}$ there are other curves, inside and outside, which were broken before. See Figures 5 and 6. For $k > k_{c,1/4}$, before penetrating through the narrow gaps of the "last created" Cantor set, they should enter the previously created Cantor sets, spend some time around the remnant islands, etc. This collective phenomenon, denoted as stickiness, tells us that it is difficult to approach an island from outside: there are several gaps to cross. But when the orbit is inside it can remain there for a long time. Upper bounds on the speed of diffusion go back to the pioneer work of Nekhorosev [32], where the author assumed that no channels of dynamics blocked at resonance exist, a requirement which is formulated in terms of a steepness condition. Similar bounds, based on estimates of the remainder of the normal form around a totally elliptic fixed point with an application to the triangular Lagrangian points can be found in [10]. For multiple examples, discussions on fast and slow escape and many illustrations on the dynamics, see [5].

These collective effects can be seen in the linear behavior (in $\log_{10} - \log_{10}$ scale) of part of the plot shown in Figure 15.

6.2 Determining additional numerical information

From the last numerical simulations in Section 5, more concretely, the ones illustrated in Figure 13, for $N = 10^5$ and $T = 2^{30}$, we can extract valuable additional information. We have collected data on the "trips" of the N initial points. In particular the residence time in the $\mathcal{W}_{E_+}$ and $\mathcal{W}_{E_-}$ domains. That is, when we have detected that an iterate approaches, say, the positive island (see end of Section 5.1), we count for how many iterates, m, it remains in $\mathcal{W}_{E_+}$ until leaving it. We introduce some intervals, of the form $I_j = [2^{j/2}, 2^{(j+1)/2})$, $j = 14, \ldots, 60$, and if $m \in I_j$ we add one unit to a counter C_j. At the end of the computations we collect the counts in each box. This gives an estimate of the average "residence time" in the vicinity of the islands.

The results are shown in Figure 15 left. In it we plot all the curves corresponding to data for $k = 1.0512(10^{-5})1.0515$ simultaneously (a total of 31 curves). For the data in each counter C_j we display, on the horizontal axis, the value of $\log_{10}(2^{j/2})$ and on the vertical axis the final value of $\log_{10}(C_j)$, adding the visits to $\mathcal{W}_{E_+}$ and $\mathcal{W}_{E_-}$. For instance we can read, from the left upper corner of the plot, that for all used values of k, the number of visits with a stay between 128 and 181 consecutive iterates exceeds the value of 10^8. Note that in very few cases the length of the "stays" exceeds the value 2^{29} and they occur, mainly, for $k = 1.05125$ and $k = 1.05126$.

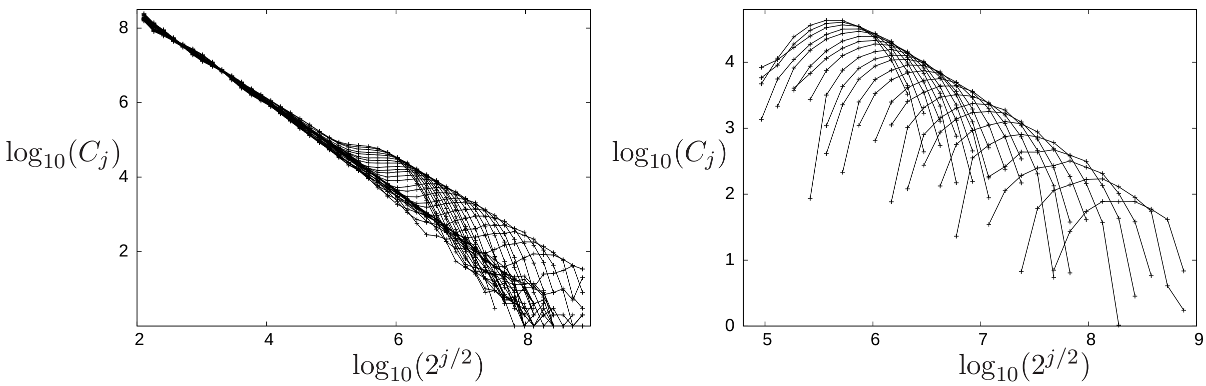

Figure 15: Left: number of times that the iterates visit $\mathcal{W}_{E_+} \cup \mathcal{W}_{E_-}$ with a stay in the range I_j as a function of $2^{j/2}$. For both variables the $\log_{10}$ scale has been used. All the values of $k = 1.05120(10^{-5})1.05150$ are plotted simultaneously. Right: A measure of the size of the bumps in the left plot. See the text for details.

In the plot we see some monotonous decrease until a value of j which depends of k. The smaller the value of k is, the larger the value of j up to which the decrease holds. For a given k, after the monotonous, close to linear, decrease until some value of j, one can see a "bump" in the value of $\log_{10}(C_j)$.

To analyze the bumps seen in Figure 15 left, we proceed as follows. For a fixed k assume that the close to linear behavior on the plot holds up to some value j_c of j. Then we do a linear fit of the data for $j \in [14, j_c]$. Note that the bumps only show up for $k > 1.05126$. Decreasing k from 1.05150 to 1.05127 the approximate values of the slopes decrease monotonically from -1.11 to -1.21. Then we subtract from the counts C_j the values predicted by the linear fit for $j > j_c$. The results are shown in Figure 15 right. Again in $\log_{10}$ scale for both variables, we plot in the horizontal direction the value of $2^{j/2}$ and in the vertical one the difference between the value of C_j and the one predicted by the fit. This is a way to obtain a qualitative representation of the behavior of the bumps in the left plot.

Note that for larger values of k the height of the bumps is larger. This is natural, because they remain for less iterates in the "linear" regime of Figure 15 left, before entering into the bump.

To study the source of the bumps, with the shape seen in Figure 15 right, we place our study in a different range of values of k for the M_k, concretely around the destruction of the last invariant rotational curve (IRC) for Greene's value $\bar{k}_G \approx 0.971635406$. The parameter in classical formulations of the standard map is denoted as $\bar{k}$, which is related to the parameter k we use in this work as $\bar{k} = 2\pi k$.

The last IRC appears for a rotation number $\rho = (\sqrt{5}-1)/2$ and, by symmetry, also for $(3-\sqrt{5})/2$. Let us denote them as the upper $\mathcal{W}_u$ and lower $\mathcal{W}_l$ last IRC. For values $\bar{k} < \bar{k}_G$ global diffusion is impossible. But for $\bar{k} > \bar{k}_G$, but close to $\bar{k}_G$, initial points located on a strip between $\mathcal{W}_u$ and $\mathcal{W}_l$ can move away.

The method given in Section 4.1.1 has been used to generate initial points in the unstable manifold of the period-2 hyperbolic orbit. Then these points are iterated until they "escape" from the previous strip. To detect the escape several methods can be used. The simplest one is to check if, in the formulation M_k of the standard map, they cross either $y = 0$ or $y = 1$. Another method looks for an approximate representation of $\mathcal{W}_u$ and then this curve is slightly shifted up (down for $\mathcal{W}_l$). When an iterate crosses some of these shifted curves it is considered as escaped. Both methods agree very well for parameters close to the critical one.

For a decreasing set of values of $\bar{k}$ tending to $\bar{k}_G$ we have taken 10^7 initial points, for every value of $\bar{k}$, and performed up to 10^{10} iterates of each of them until escape is detected. From the more than 2×10^9 initial points tested for many values of $\bar{k}$, only 46 have not yet escaped for 10^{10} iterates.

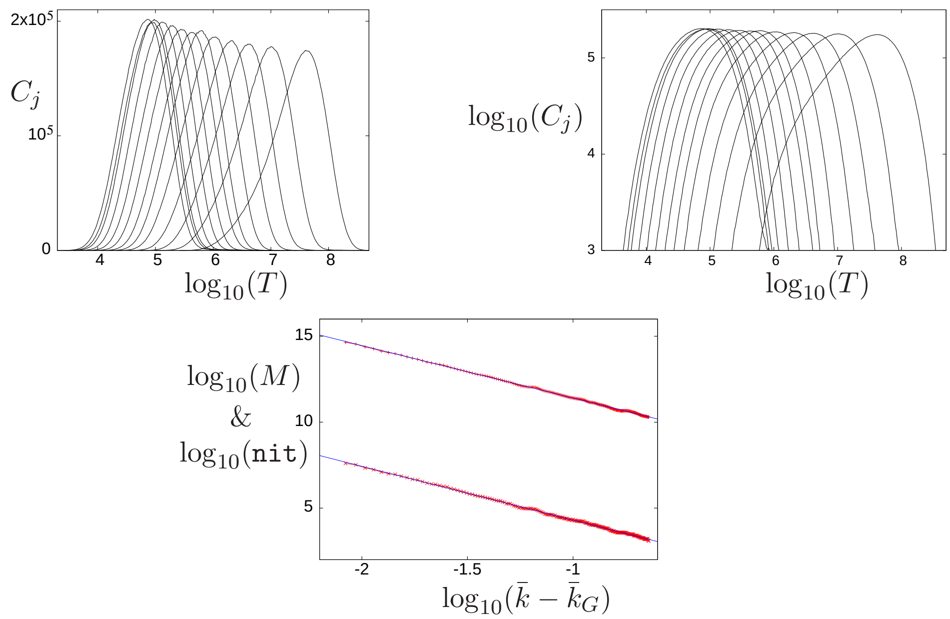

Figure 16: Statistics concerning the number of iterates to escape from an initially confined strip when the parameter $\bar{k}$ becomes larger than the critical Greene's value $\bar{k}_G$. In the top left and right plots the horizontal scale is $\log_{10}(T)$. The data on the left are represented in true scale and in the top right in $\log_{10}$ scale. Bottom: total number of iterates `nit` to have escape of all initial points (upper set) and maxima M of the previous plots (lower set), both in $\log_{10}$ scale, as a function of $\log_{10}(\bar{k}-\bar{k}_G)$. Both sets have a behavior close to linear in these scales. For these plots we have used $\bar{k} = 0.980(0.001)1.200$. See the text for additional details.

The Figure 16 shows some statistics of escapes for $\bar{k} = 0.98(0.005)1.04$. To this end we count, in a similar way to what has been described to obtain Figure 15, how many points, C_j, escape after a number of iterates T in the interval $I_j = [10^{0.02j}, 10^{0.02(j+1)})$, $j = 100, \ldots, 500$.

The top left plot in Figure 16 displays the values of C_j as a function of $0.02j$. Obviously, the closer $\bar{k}$ is to $\bar{k}_G$, the larger the number of iterates is. In the top right plot the representation is similar, but instead of C_j we display $\log_{10}(C_j)$. From one side, it is remarkable to see that, beyond a shift and a small deformation, the curves are very similar. On the other hand there is a strong similitude between the middle plot and the one that we have seen in Figure 15. This shows that the bumps in Figure 15 are due to the effect of the cantori gaps surrounding the stability regions of E_+ and E_-. See Section 6.1 for further details.

To complete the information displayed in Figure 16, top plots, we can display, as a function of $\log_{10}(\bar{k}-\bar{k}_G)$, both the total number of iterates to have escape of (essentially) all the points, and the location of the maxima in the previous two plots, both numbers in $\log_{10}$ scale. This is shown in Figure 16 bottom. The straight lines show the corresponding linear fits. The slope for the upper data (iterates) is ≈ -3.05 while the one for the lower data (maxima) is ≈ -3.13. They are in good agreement with the expectations from renormalization theory around the golden rotation number curve breakdown, see Section 6.4, specially with (13).

For completeness we have also computed, from the data shown in Figure 16, the average and standard deviation of the number of iterates to escape, as a function of $\bar{k}$. We found a good agreement with a power law of the form $(\bar{k}-\bar{k}_G)^{-\beta}$, for the value of β in (13), both for the mean and for the standard deviation. Furthermore, as it is well-known from renormalization theory [21], these two values tend to coincide when $\bar{k}$ tends to $\bar{k}_G$ and the numerical computations show this tendency.

We return now to $\bar{M}_k$ for k slightly greater than 1, with the same set of values of k used in Figure 13 right and in Figure 15. As mentioned in Section 5.1 we can count how many times a temporary capture, i.e., entrance in $\mathcal{W}_{E_+}\cup\mathcal{W}_{E_-}$, is produced. This can be divided by the total number of iterates ($10^5\times 2^{30}$ for each value of k). This gives an estimate of the probability that a point in the chaotic domain is temporary captured by an island. The results are represented in Figure 17 top left as a function of k.

On the other hand we can check how many iterations are spent in these temporary captures. The results are shown in Figure 17 top middle. Note, however, that for the contribution to the standard deviation $\sigma_{T,k}$ for the present $T=2^{30}$ it is not just the total number of iterates in $\mathcal{W}_{E_+}\cup\mathcal{W}_{E_-}$ what matters, but how long are the "stays" near the islands. A stay 10^6 units long counts as much as 100 stays 10^5 units long. Furthermore, to check that what really matters are the iterates and "stays" in $\mathcal{W}_{E_+}\cup\mathcal{W}_{E_-}$, for the set of values of k used in Figure 17, we have computed the standard deviation looking only to the stays in $\mathcal{W}_{E_+}\cup\mathcal{W}_{E_-}$. Concretely, if some initial point has visited m_+ times $\mathcal{W}_{E_+}$ and m_- times $\mathcal{W}_{E_-}$, it contributes as m_+-m_- to the computation of the standard deviation. All the iterates in the chaotic domain are discarded. The values of the $\sigma_{T,k}$ computed in that way have a relative error below 0.0005 with respect to the correct values for $k=1.05120(0.00001)1.05150$.

Finally we plot at the top right part of Figure 17 the evolution of the estimated value of the non-normalized standard deviation $\sigma_T(k)$, see (12), as a function of T for the values of k used to produce Figure 13 right. We use $\log_{10}$ scales. Globally one can see that up to $T\approx 10^4$ the behavior is close to linear, with a slope larger than 1/2. Concretely, it is close to 0.63, due already to the effect of the points near the islands. From that value of T on, there is a change and the values of $\sigma_T(k)$ lie between two lines of slopes 0.7 and 1, say the lower and the upper lines. If we look at the individual behavior of the lines for the different values of k, see the details in the magnification shown in the bottom plot, it is checked that up to $k=1.05123$ the curves stay near the lower line. For $k=1.05124$ the curve ends in the middle of the lower and upper lines, with $\sigma_T(k)\approx 10^7$ for $T=2^{30}$. For $k=1.05126$ it reaches the upper line at the end of the T domain. From that value of k on, the curve has a tangency with the upper line, for values of T which decrease as k increases (compare with

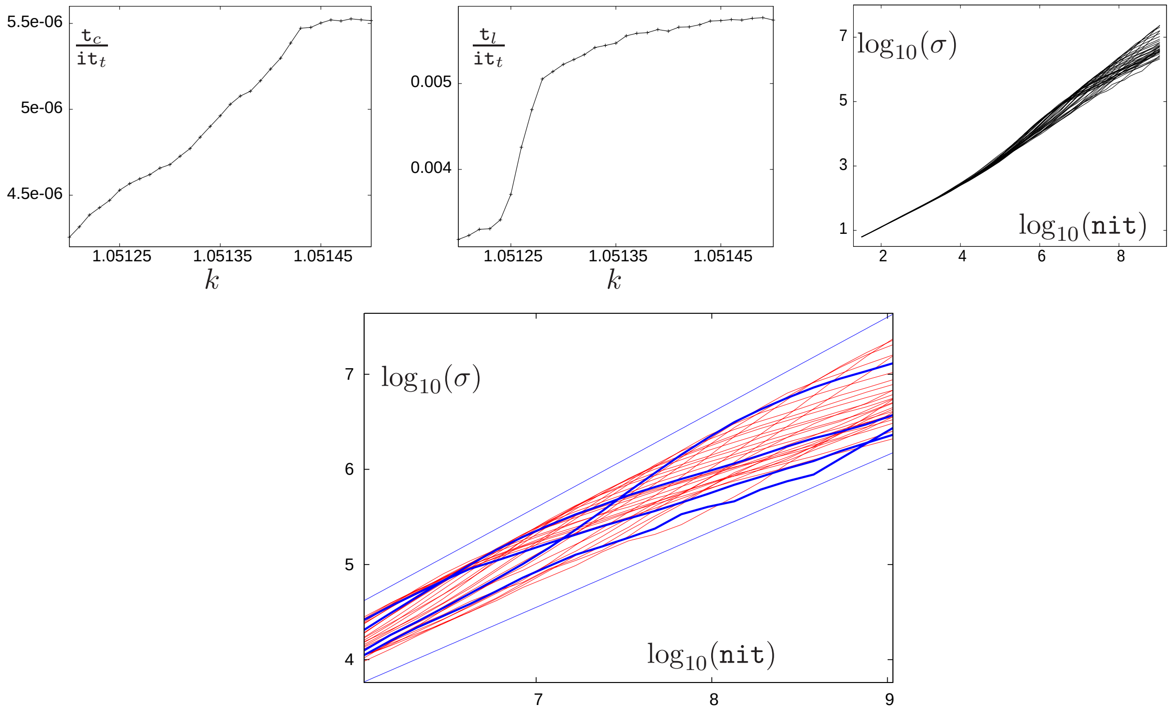

Figure 17: Top left: Number of temporary captures $\mathtt{t}_c$ in the $\mathcal{W}_{E_+} \cup \mathcal{W}_{E_-}$ domains divided by the total number $\mathtt{it}_t$ of iterates of all the initial points. Top middle: total lengths $\mathtt{tl}$ of the stays near islands divided by the same quantity. Both data are represented as a function of k. Top right: For all the k values of the previous plots the standard deviation σ is represented as a function of the number $\mathtt{nit}$ of iterates in $\log_{10}$ scale. Bottom: A magnification of the top right plot for $\mathtt{nit}$ between 2^{20} and 2^{30} with the lines for $k = 1.0512(0.0001)1.0515$ shown as thick blue lines. For reference two straight lines with slopes 0.7 and 1, mentioned as lower and upper lines in the text, are also shown.

Figure 15), and then it decreases approaching the lower curve. The curves shown with thick blue lines illustrate this behavior.

Up to this point we have commented on the numerical results obtained. These results show that for a generic area-preserving map with a divided phase space the diffusion properties are far from trivial. Despite of the difficulties, and motivated by the interest in applications, many authors have investigated the diffusive properties both from numerical and theoretical points of view. Next subsection relates the numerical results obtained with the available theoretical approaches to the diffusive properties in the different regimes observed.

6.3 Available theoretical frameworks from renormalization schemes

In what follows we briefly present the theoretical frameworks that either support or even explain some of the numerical results shown.

The correlation function is related to the probability $P^e(t)$ of leaving a fixed region of the phase space in time t. To fix ideas, consider the accelerator mode islands of M_k. The probability $P^e(t)$ relative to these islands was shown in Figure 15 left. First we note that in a purely diffusive regime the correlation function decays exponentially in time, see [19] and references therein ("time" here means "number of iterates of the map"). That would mean that the points can escape from the chaotic region region easily as time evolves. However, we observed a power-law decay of P^e for the region. Similar results were obtained in many other works, see [2, 3, 4, 16] for example. This means that trajectories are expected to be for a large number of iterates in the neighbourhood of the accelerator mode island, as confirmed by the numerical experiment in Section 5. See also [8, 9] for more recent computations on the statistics of the Poincaré recurrences using the Ulam method.

What causes the power-law decay and the stickiness effect has been analysed from different points of view. The analysis performed in [2] derived a power-law behaviour in terms of the non-homogeneous diffusion coefficient $D(y)$ of the separatrix map. The analysis of self-similar solutions of the diffusion equation (which was suggested to include a suitable exponent α) lead to the power-law probability distribution. This self-similarity was then related with suitable scalings in time and space of the island-around-island structure, meaning that for long-time evolution is this hierarchy the responsible of the behaviour of P^e. Further developments of this point of view were done by Zaslavsky and collaborators, giving rise to a renormalization approach related to the hierarchical islands, see [44]. Let us give some details of this approach.

The presence of accelerator modes causes the divergence of the diffusion coefficient since the variance of a power-law distribution grows to infinity. Assume that the density of probability is of the form $f_{P^e} \sim a/T^b$. For $2 < b \leq 3$ the expected value exists but the variance diverges. According to the Zaslavsky renormalization scheme, see [45], one has

$$b = 1 + \frac{\log \lambda_s}{\log \lambda_T},$$

where λ_s is the corresponding scaling factor of the area of two consecutive islands in the hierarchical structure and λ_T is the scaling factor related to the period of the last invariant curves of these islands. These scalings are assumed to hold approximately and obtained from computations of the first islands in the structure. Several computations for the web map and the standard map for different hierarchies of islands show that $b \approx 2.2$. It is worth noting that the same factor was numerically observed in [27] for the Mather's ΔW [26] measured in different consecutive islands of a hierarchy (referred there by a class, see [27]), concretely it was observed that $\Delta W_c = \Delta W_{c-1} q^{-\psi}$, with $\psi = 2.2$ and where p/q, $p, q \in \mathbb{Z}$ is the frequency of the periodic point of the class c orbit. We refer to [45] and references therein for further details. On the other hand, in [45] it was also observed that the variance of the fractional Fokker-Planck-Kolmogorov equation

$$\frac{\partial^\beta f}{\partial t^\beta} = \frac{1}{2} \frac{\partial^\alpha}{\partial(-x)^\alpha} \left(\frac{\partial^\alpha (Bf)}{\partial(-x)^\alpha} - \frac{\partial^\alpha B}{\partial(-x)^\alpha} f \right),$$

behaves like $t^{\beta/\alpha}$, which provides an explicit relation with the scalings λ_s and λ_T of the renormalization scheme. Further discussions on scaling laws can be found in [43].

In our experiments we also observed the stickiness effect of cantori. To analyse this phenomenon MacKay in [20], and in an extended version in [21], defines a renormalization operator in a class of area preserving twist maps. Let ω be an irrational number whose continued fraction expansion and rational convergents are

$$\omega = a_0 + 1/(a_1 + 1/(a_2 + \cdots)) \equiv [a_0, a_1, a_2, \ldots], \quad a_i \geq 1, i > 0; \quad p_n/q_n = [a_0, \ldots, a_n].$$

Then $p_n/q_n \to \omega$ as $n \to \infty$. Let $F_\mu : (I, \theta) = (\bar{I}, \bar{\theta})$ be a twist APM 1-periodic in θ and having a critical invariant circle of rotation number ω for $\mu = 0$, and $R(I, \theta) = (I, \theta - 1)$. The results obtained suggest that there are scalings B_n such that the sequence

$$B_n^{-1} F^{q_n}_{\mu\delta^{-n}} R^{p_n} B_n$$

converges to a universal map $F^\star$, where $B_n \simeq BB_{n-1}$, $B(x,y) = (\alpha x, \beta y)$ and it does geometrically with ratio $1/\delta$. In particular he did computations for noble rotation numbers, that is, for which $a_i = 1$ for $i > i_0, i_0 \geq 0$ obtaining

$$\delta = 1.62795, \qquad \alpha = -1.4148360, \qquad \beta = -3.0668882\,. \tag{13}$$

The impact of these results in transport properties of the map in the vicinity of the just broken invariant circle are worth noting. One of the consequences of these scalings is that Mather's ΔW [26] scales as follows. If Δk is some small quantity,

$$\Delta W_\omega(k_c + \Delta k/\delta) \approx \Delta W_\omega(k_c + \Delta k)/(\alpha\beta),$$

so that there exists a 1-periodic universal function $U(x) = U(x+1)$ such that

$$\Delta W_\omega(k_c + \Delta k) \approx A(\Delta k)^B U(\log_\delta(\alpha\beta)), \qquad B = \log_\delta(\alpha\beta) \approx 3.0117220\,.$$

This quantity $\Delta W_{(p/q)}$, as is proved in [22] is exactly the *flux*, the area per iterate that crosses through the gaps in a periodic orbit, and ΔW_ω is the area that crosses through a cantorus (when it is an invariant curve the flux is zero, as expected). As a function of the parameter k in the case of M_k (3), the time to cross an invariant Cantor set $\langle N\rangle(k)$, conditioned to do it eventually, is related to the flux and the accessible area $\mathcal{A}(k)$ via the Kac formula [28]

$$\langle N\rangle(k) \times \Delta_\omega W(k) = \mathcal{A}(k),$$

where $\mathcal{A}(k)$ can be assumed to be bounded between two close positive constants for small enough variations of k so that the time to cross an Aubry-Mather set, sufficiently close to the breakdown, behaves as

$$\langle N\rangle(k) \sim \frac{1}{\Delta k^B},$$

where $\log_\delta$-periodic fluctuations are expected. Note that this law is exactly the same observed by Chirikov in [1]. In order to be able to use this approach to the escape from an island, the effects of islands-around-islands should be included, as in the Markov tree model in [30].

6.4 Comparing with limit theoretical predictions

Now we are in situation to explain the changes observed on the behavior of the standard deviation, for different values of k, T and N, at the light of the previous theoretical considerations.

For a given initial point, located in the chaotic domain, there is some small probability, say ε_1, to enter $\mathcal{W}_{E_+} \cup \mathcal{W}_{E_-}$. This is illustrated in Figure 17 left. Note that even for $k < k_{c,1/4}$ one has $\varepsilon_1 > 0$. The iterates can enter in $\mathcal{W}_{E_+}$, say, but can not cross the still existing invariant curves. Increasing k the value of ε_1 increases up to some saturation. This is due to the fact that the gaps of the more external cantori are larger.

For $k < k_{c,1/4}$ the only contribution to $\sigma_T(k)$ is the "residence" in $\mathcal{W}_{E_+}$ but outside the invariant curves. Hence, the values of the standard deviation, either scaled or not, are not so large, as illustrated in Figure 13 (skip the effect of the small peaks). According to [45] one should have a power law with exponent ≈ -2.2 in the residence time inside $\mathcal{W}_{E_+}$. Here the power refers to the one in the probability density function (pdf) of the residence time near islands. This is illustrated in Figure 15. In the fits of the corresponding cumulative distribution functions (cdf) we did, to "extract" the bumps, we found slopes that were tending to -1.21 when $k > k_{c,1/4}$ was approaching $k_{c,1/4}$. But in Figure 15 we show results for iterates in a sample with constant step in $\log_{10}$ scale. That is, not for a value of the number of iterates but for a range of fixed amplitude in log scale. This means that in the true iterate scale the exponent of the pdf of the residence time near islands is close to -2.21, in very good agreement with [45].

Now assume $k > k_{c,1/4}$. Immediately after $k_{c,1/4}$ the gaps on the Cantor set which replaces the last invariant curve (that we denote in what follows as the last Cantor), are so small that they produce almost no effect. This can be seen, both in Figure 15, where the bumps displayed on the right start at $k = 1.05127$, and in description of the bottom plots in Figure 17.

Further increase of k leads to an increased probability to enter inside the last Cantor. When inside, they remain there for an average number of iterates of the form $c(k - k_{c,1/4})^\beta$ for some $c > 0$ and β as given in (13). For a given T there exists a value of k, say $k^*(T)$ such that the mean residence time inside the last Cantor equals T. In other words: some points enter inside that Cantor and for the full number of iterates they remain inside. The final value of the jump $\Delta^T y = y_T - y_0$ equals T. Even if the fraction of points is not so large, there is a contribution to $\sigma_T(k)$ of the order of T.

Increasing k from $k^*(T)$ on, should produce a decrease in $\sigma_T(k)$, because the probability to enter the last Cantor is larger, the mean residence time is less or much less than T. Hence, the "large contributions" to $\sigma_T(k)$ are no longer present. It is clear that the iterates of a point which enter the last Cantor and leave it, can reenter later (after many additional iterations), but the global effect will be less important. One would need many more iterates (i.e., a larger T) and this will decrease the slope in Figure 17 bottom plots.

This reasoning also explains the tangencies mentioned concerning Figure 17 bottom, specially in the right one. When k increases, the value of T at the tangency decreases: the function $k^*(T)$ decreases if T increases and tends to $k_{c,1/4}$ when $T \to \infty$. This is also related to the fact that, in many previous figures, using the scaled standard deviation, the maximum appears multiplied by a factor γ when T is increases by a factor γ^2.

Finally we can comment on the behaviour of $\sigma_T(k)$, for a fixed k around $k_{c,1/4}$ for very large values of T, producing a lower bound of the standard deviation. We start by stating several simplifying assumptions. For concreteness we denote the domain $\mathcal{W}_{E_+} \cup \mathcal{W}_{E_-}$ as the islands zone, and the complement as the chaotic zone.

a) A point in the chaotic zone has a probability $1 - \varepsilon$ to remain on it after one iteration and equal probabilities, $\varepsilon/2$, to enter $\mathcal{W}_{E_+}$ or $\mathcal{W}_{E_-}$. Hence, to remain for m consecutive iterations in the chaotic zone and then to enter into the islands zone, one has a probability $(1 - \varepsilon)^m \varepsilon$. Both the average and standard deviation are $1/\varepsilon + \mathcal{O}(1)$. According to the data in Figure 17 top left, the values of ε for k around $k_{c,1/4}$ are close to 5×10^{-6}.

b) A point which has entered into the islands zone remains on it at least for m_0 iterates. The probability to go out after $m > m_0$ iterates is of the form c/m^b where $c > 0$ and $2 < b < 3$. From the normalization, requiring $\int_{m_0}^{\infty} cm^{-b}\, dm = 1$, it follows $c = (b-1)m_0^{b-1}(1 + o(1))$. The distribution has average $\approx \frac{b-1}{b-2} m_0$. The value of b can be estimated from Figure 15 to be around 2.2 and m_0 can then be estimated from the average length of the stays in the islands zone, which follows from the plots in Figure 17 top, and the expression above for the average. The values of m_0 derived in this way range from 128 to 170, approximately.

   The probability that the number of iterates in the islands exceeds a value M follows easily and it is given by $(m_0/M)^{b-1}$. We recall, as already said, that the variance of this distribution becomes unbounded.

c) We assume that the different events (remaining in the chaotic zone, entering one or the other islands zones and remaining a given number of iterates on it) are independent. As commented in subsection 4.2 and illustrated in Figure 8, this is not true, but the correction factor obtained for the diffusion coefficient due to the correlation is not too far from one.

Under the above assumptions one has the following

Proposition 2. *The standard deviation of a sample of initial points after T iterations, with T large enough, is bounded from below by $T^{2-(b+1/b)/2}$.*

Proof. Let $\gamma > 0, \delta > 0$, to be selected during the proof. We consider the iteration of a given initial point. Assume, first, that until an iterate such that the total number of iterates in the chaotic zone is T^γ, all the entrances in the islands zones have lengths bounded by T^δ until a long stay entrance occurs.

Applying the central limit theorem to the distribution in the chaotic zone, one has that the number of times that an iterate enters the islands zone is $\varepsilon T^\gamma(1+o(1))$. The probability that in each one of the stays in the islands zone the number of iterates in the island is bounded by T^δ is bounded by

$$\left[1-\left(\frac{m_0}{T^\delta}\right)^{b-1}\right]^{\varepsilon T^\gamma}(1+o(1)),$$

which behaves like $\exp(-\varepsilon m_0^{b-1}T^{\gamma-\delta(b-1)})$, that is, very close to 1 if $\gamma-\delta(b-1)\leq 0$ for the ranges of ε, m_0, b that we are considering.

Now assume that a long stay in the islands zone occurs and the point remains there for, at least, T iterates. The probability is $(m_0/T)^{b-1}$. It is clear that the computation is stopped as soon as the total number of iterates exceeds T. The number of possibilities of such event to occur is $\varepsilon T^\gamma(1+o(1))$. If we assume that this long stay occurs in the positive island, even if the other stays are in the negative one, and neglecting the contribution $\mathcal{O}(T^{\gamma/2})$ due to the stays on the chaotic zone, for the final value of $|y|$ one has a value bounded from below by $T-2\varepsilon T^\gamma T^\delta(1+o(1)) > 0.999T$, provided $\gamma+\delta\leq 1$.

The contribution to the sum of squares of the changes in y is bounded from below by

$$\varepsilon T^\gamma(1+o(1))\left(\frac{m_0}{T}\right)^{b-1}(0.999T)^2. \tag{14}$$

From the conditions for γ, δ one has that the optimal choice is obtained if $\gamma=\delta(b-1)$, $\gamma+\delta=1$, which gives as exponent of T in (14) equal to $4-b-1/b$. By the assumptions on the equal probabilities to enter $\mathcal{W}_{E_+}$ or $\mathcal{W}_{E_-}$, the average of y is negligible in front of this quantity and the Proposition follows. □

Figure 18 shows an illustration similar to Figure 17 bottom, for $k = 1.0515$, a number of initial points $N = 10^4$ and a final number of iterations $T = 2^{40}$. For reference a line with slope 0.7 is also shown. We note that, assuming $b = 2.2$, the lower limit of the slope predicted by proposition 2 is ≈ 0.673. The contributions of other stays in the islands zones are responsible of the difference of limit slopes for T very large. We should mention that for $T = 2^{38}$ and $T = 2^{39}$ the results are below what we expected, while for $T = 2^{40}$ are a little bit larger than expected. Looking at the behavior of the iterates of the initial points one checks that for $T = 2^{38}, 2^{39}$ the largest values of $|y|$ are slightly larger than 1.1×10^9, a little bit more than the value already reached for $T = 2^{37}$ iterates. On the other hand, for $T = 2^{40}$ one of the points reaches $y = 1.327\times 10^{10}$. This single point gives half of the total contribution to σ. But this anomaly is nothing else than a consequence of the reduced size of the sample.

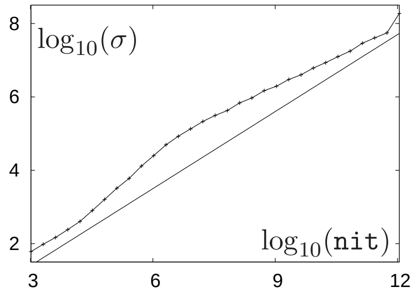

Figure 18: The standard deviation σ as a function of the number of iterates T for $k = 1.0515$, for large values of T. Both variables shown in $\log_{10}$ scale.

7 Conclusions

In this paper we have presented several numerical massive experiments concerning the non-homogeneous diffusion properties of area preserving maps. Concretely we have focused on the Chirikov standard map for (relatively) large values of the parameter. The obtained results show the relevant role of the accelerator mode islands, whose local properties in the highly chaotic regime of the standard map have been related with those of the Hénon map. The effect of cantori and islands-around-islands structures surrounding these accelerator modes on the regular diffusion characteristics has been analysed.

The normal diffusive behaviour observed for most of the parameter values no longer persists for ranges at which sticky structures appear. In particular, our results confirm the power-law decay in time of the probability of being trapped in an islands-around-islands hierarchical structure. Furthermore, a different power-law decay in time, produced by the effect of cantori gaps, has been also detected for some parameters. Both situations have a theoretical framework which reasonably explain the results. In fact, it is possible to understand the numerical results at the light of the limit cases described by the available theories.

However, it would be of great interest for applications to be able to predict which of these different regimes dominates for a given parameter value, hence being the mechanism responsible of the expected average diffusion properties of the system. Furthermore, the validity limits (either in phase space and/or parameter space) of the (quantitative) data predicted by the theoretical approaches should be also investigated. It seems that some part of the information required to make quantitative predictions valid for large domains in the phase+parameter space requires some preliminary numerical experiments. These questions will be considered elsewhere.

Acknowledgments

The authors have been supported by grants MTM2010-16425 (Spain) and 2009 SGR 67 (Catalonia). We thank Jaume Timoneda for the maintenance task of the computing facilities of the Dynamical Systems Group of the Universitat de Barcelona, that have been largely used in this work, up to a total of floating point operations which exceeds 5 exaflop. The authors also want to thank Robert MacKay and Vered Rom-Kedar for helpful discussions on related topics.

References

[1] Chirikov, B.V., A universal instability of many-dimensional oscillator systems, *Phys. Rep.*, 1979, Vol. 52, no. 5, pp. 264–379.

[2] Chirikov, B.V., Chaotic dynamics in Hamiltonian systems with divided phase space. In *Proceed. Sitges Conference on Dynamical Systems and Chaos*, Garrido, L., editor, Lecture Notes in Physics, Vol. 179, Springer, 1983.

[3] Chirikov, B.V. and Shepelyansky, D.L., Statistics of Poincaré recurrences and the structure of the stochastic layer of a nonlinear resonance, Ninth international conference on nonlinear oscillations, Vol. 2 Kiev, 1981. Translation to English: Plasma physics laboratory, Princeton University, 1983.

[4] Chirikov, B.V. and Shepelyansky, D.L., Correlation properties of dynamical chaos in Hamiltonian systems, *Physica D*, 1984, no. 13, pp. 395–400.

[5] Contopoulos, G. and Harsoula, M., Stickiness effects in conservative systems, *Internat. J. Bifur. Chaos Appl. Sci. Engrg.*, 2010, Vol. 20, no. 7, pp. 2005–2043.

[6] Duarte, P., Plenty of elliptic islands for the standard family of area preserving maps, *Ann. Inst. H. Poincar Anal. Non Linaire*, 1994, Vol. 11, no. 4, pp. 359–409.

[7] Dumortier, F., Ibáñez, S. et al, About the unfolding of a Hopf-zero singularity, *Discrete Contin. Dyn. Syst. Ser. A*, 2013, Vol. 33, pp. 4435–4471.

[8] Frahm, K.M. and Shepelyansky, D.L., Ulam method for the Chirikov standard map. *Eur. Phys. J. B*, 2010, Vol. 76, pp. 57–68.

[9] Frahm, K.M. and Shepelyansky, D.L., Poincaré recurrences and Ulam method for the Chirikov standard map. *Eur. Phys. J. B*, 2013, Vol. 86, pp. 322–333.

[10] Giorgilli, A., Delshams, A. et al, Effective stability for a Hamiltonian system near an elliptic equilibrium point, with an application to the restricted three body problem. *J. Diff. Eq.*, 1989, Vol. 77, 167–198.

[11] Gonchenko, M., *Homoclinic phenomena in conservative systems*, Ph.D. Thesis, Universitat Politècnica de Catalunya, 2013.

[12] Gonchenko, S.V. and Shilnikov, L.P., On two-dimensional area-preserving mappings with homoclinic tangencies, *Russian Math. Dokl.*, 2001, Vol. 63, no. 3, pp. 395–399.

[13] Greene, J.M., A method for determining stochastic transition. *J. Math. Phys.*, 1979, Vol. 6, no. 20, pp. 1183–1201.

[14] Hénon, M., Numerical study of quadratic area-preserving mappings, *Quart. Appl. Math.*, 1969, Vol. 27, pp. 291–312.

[15] Jungreis, I., A method for proving that monotone twist maps have no invariant circles. *Ergod. Th. & Dynam. Sys.*, 1991, Vol. 11, 79–84.

[16] Karney, C.F.F., Long time correlations in the stochastic regime, *Physica D*, 1983, Vol. 3 no. 8, pp. 360–380.

[17] Karney, C.F.F., Rechester, A. and White, B., Effect of noise on the standard mapping, *Physica D*, 1982, Vol. 4, no. 3, pp. 425–438.

[18] Ledrappier, F., Shub, M. et al, Random versus deterministic exponents in a rich family of diffeomorphisms, *J. Stat Phys.*, 2003, Vol. 113, pp. 85–149.

[19] Lichtenberg, A.J. and Lieberman, M.A., *Regular And Chaotic Dynamics*, Applied Mathematical Sciences, 2nd edition, Springer, New York, 1992.

[20] MacKay, R.S., A renormalisation approach to invariant circles in area-preserving maps. *Physica D*, 1983 Vol. 7, no. 1-3 pp. 283–300. Order in chaos (Los Alamos, N.M., 1982).

[21] MacKay, R.S., *Renormalisation in area-preserving maps.* Advanced Series in Nonlinear Dynamics, 6. World Scientific. 1992

[22] MacKay, R.S., Meiss J.D. and Percival, I., Transport in Hamiltonian systems. *Physica D*, 1984 Vol. 13, no. 1-2 pp. 55–81.

[23] MacKay, R.S. and Percival, I.C., Converse KAM: theory and practice. *Comm. Math. Phys.* 1985 Vol. 98 no. 4 pp. 469–512.

[24] Mackay, R.S. and Stark, J., Locally most robust circles and boundary circles for area-preserving maps. *Nonlinearity*, 1992, Vol. 5, pp. 867–888.

[25] Marmi, S. and Stark, J., On the standard map critical function. *Nonlinearity*, 1992, Vol. 5, pp. 743–761.

[26] Mather, J.N., Nonexistence of invariant circles. *Ergod. Th. & Dynam. Sys.*, 1984, Vol. 4, no. 2, pp. 301–309.

[27] Meiss, J.D., Class renormalization: Islands around islands, *Phys. Rev. A*, 1986, Vol. 34, no. 3 , pp. 2375–2383.

[28] Meiss, J.D., Average exit time for volume-preserving maps. *Chaos*, 1997 no. 7, pp. 139–147

[29] Meiss, J.D., Cary, J.R. et al, Correlations of Periodic Area-Preserving Maps, *Physica D*, 1983, Vol. 6, no. 3, pp. 375–384.

[30] Meiss, J.D. and Ott, E., Markov tree model of transport in area-preserving maps. *Physica D*, 1986 Vol. 20, no. 2-3, pp. 387–402

[31] Miguel, N., Simó, C. and Vieiro, A., From the Hénon conservative map to the Chirikov standard map for large parameter values, *Regular and Chaotic Dynamics*, 2013, Vol. 20, 469–489.

[32] Nekhorosev, N.N., An exponential estimate of the time of stability of nearly-integrable Hamiltonian systems. *Russian Mathematical Surveys*, 1977, Vol. 32, pp. 1–65.

[33] Olvera, A. and Simó, C., An obstruction method for the destruction of invariant curves. *Physica D*, 1987, Vol. 26, pp. 181–192.

[34] Pesin, Ya., Characteristic exponents and smooth ergodic theory, *Russian Math. Surveys*, 1977, Vol. 32, pp. 55–114.

[35] Rom-Kedar, V. and Zaslavsky, G., Islands of accelerator modes and homoclinic tangles. *Chaos*, 1999, Vol. 9. no. 3, pp. 697–705.

[36] Sánchez, J., Net, M. and Simó, C., Computation of invariant tori by Newton-Krylov methods in large-scale dissipative systems, *Physica D*, 2010, Vol. 239, pp. 123–133.

[37] Simó, C., Analytical and numerical computation of invariant manifolds. In *Modern methods in celestial mechanics*, Benest, D. et Froeschlé, C., editeurs, Editions Frontières, 1990, pp. 285–330.

[38] Simó, C. Some properties of the global behaviour of conservative low dimensional systems. In *Foundations of Computational Mathematics: Hong Kong 2008*, Cucker, F. et al. editors, London Math. Soc. Lecture Notes Series, Vol. 363, pp. 163–189, Cambridge Univ. Press, 2009.

[39] Simó, C., Sousa-Silva, P. and Terra, M., Practical Stability Domains near $L_{4,5}$ in the Restricted Three-Body Problem: Some preliminary facts. In "Progress and Challenges in Dynamical Systems" Vol. 54, Springer, 2013, pp. 367–382.

[40] Simó, C. and Vieiro, A., Resonant zones, inner and outer splittings in generic and low order resonances of Area Preserving Maps, *Nonlinearity*, 2009, Vol. 22, pp. 1191–1245.

[41] Simó, C. and Vieiro, A., Dynamics in chaotic zones of area preserving maps: close to separatrix and global instability zones, *Physica D*, 2011, Vol. 240, no. 8, pp. 732–753.

[42] Venegeroles, R., Calculation of superdiffusion for the Chirikov-Taylor model, *Physical Review Letters*, 2008, 101(5): 054102.

[43] Venegeroles, R., Universality of Algebraic Laws in Hamiltonian Systems, *Physical Review Letters*, 2009, 102(6): 064101.

[44] Zaslavsky, G.M., Dynamical traps. *Physica D*, 2002, Vol. 168-169, pp. 292–304.

[45] Zaslavsky, G.M., Edelman, M. and Niyazov, B.A., Self-similarity, renormalization, and phase space nonuniformity of Hamiltonian chaotic dynamics. *Chaos*, 1997, Vol. 7, no. 1, pp. 159–181.